Title

Advancing Tools for Treating Usher Syndrome 1B and Elucidating the Role of Myosin VIIa in the Retinal Pigment Epithelium

Author

Gilmore, William Blake

Publication Date

2023

Peer reviewed|Thesis/dissertation

UNIVERSITY OF CALIFORNIA

Los Angeles

Advancing Tools for Treating Usher Syndrome 1B and Elucidating the Role of Myosin VIIa in the Retinal Pigment Epithelium

A dissertation submitted in partial satisfaction of the

requirements for the degree Doctor of Philosophy

in Molecular and Medical Pharmacology

by

William Blake Gilmore

2023

ABSTRACT OF THE DISSERTATION

Advancing Tools for Treating Usher Syndrome 1B and Elucidating the Role of Myosin VIIa in the Retinal Pigment Epithelium

by

William Blake Gilmore

Doctor of Philosophy in Molecular and Medical Pharmacology

University of California, Los Angeles, 2023

Professor David S. Williams, Co-Chair

Professor Caius Radu, Co-Chair

Usher Syndrome 1B (USH1B) is a severe genetic disorder characterized by congenital deafness and progressive vision loss due to retinitis pigmentosa. The role of myosin VIIa in the retinal pigment epithelium (RPE) is critical for photoreceptor function and survival, and mutations in the myosin VIIa gene (MYO7A) are the primary cause of USH1B. This work aims to advance therapeutic tools for USH1B and introduce tools that shed light on the functional roles of myosin VIIa within the RPE. We employed

novel gene editing tools to correct Myo7a mutations using an engineered cell line. This cell line can be used as a cost-effective high-throughput approach for screening guide RNA sequences for producing precise gene edits. Additionally, we developed and optimized gene vectors for efficient delivery of the base editing system to disease models. This work focused on restoring functional myosin VIIa protein expression in the shaker-1 mouse, an animal model of USH1B. Our results highlight the promise of base editing for advancing approaches in gene therapy, and introduce a novel set of tools for better exploring the biological roles of myosin VIIa.

The dissertation of William Blake Gilmore is approved.

Ajit Divakaruni

Roxana Radu

Caius Radu, Committee Co-Chair

David S. Williams, Committee Co-Chair

TABLE OF CONTENTS

LIST OF FIGURES AND TABLES

LIST OF ABBREVIATIONS AND SYMBOLS

AAV	Adeno-associated virus
BRB	Blood-retinal barrier
DSB	Double stranded break
GCL	Ganglion cell layer
DHA	Docosahexaenoic acid
ECM	Extracellular matrix
ESC	Embryonic stem cell
iPSC	Induced pluripotent stem cells
INL	Inner nuclear layer
MYO7A	Human myosin VIIa gene
Myo7a	Mouse myosin VIIa gene
NFL	Nerve fiber layer
OLM	Outer limiting membrane
OPL	Outer plexiform layer
ONL	Outer nuclear Layer
PEDF	Pigment epithelial derived factor
PS	Phosphatidylserine
pA	Polyadenylation signal
POS	Photoreceptor outer segment
RP	Retinitis pigmentosa

RPE	Retinal pigment Epithelium
TALEN	Transcription activator-like effector nuclease
USH	Usher syndrome
USH1B	Usher syndrome type 1B
VEGF	Vascular endothelial growth factor
WT	Wildtype
ZFN	Zinc finger nuclease

ACKNOWLEDGEMENTS

This work was supported by NIH NEI grants R01EY027442, R01EY033035, R21EY031109 and P30EY00333, and a program project grant from the Foundation Fighting Blindness (DSW); by NIH NEI postdoctoral fellowship F32EY031575 (NWH); and by the Gates Frontiers Fund, The Solich Fund, *CellSight* Development Fund, and an unrestricted grant to the Department of Ophthalmology, University of Colorado from Research to Prevent Blindness (MVCS).

Chapter 1 of this dissertation represents the publication in Vision Research (Gilmore et al., 2023), with individual contributions noted in the publication. The work described in Chapter 2 was inspired by constructs provided by José S Ramalho, PhD, Principal Investigator at Universidade NOVA de Lisboa, Lisboa, Portugal. Preliminary validation of the tools described in this chapter was performed by Gil Torten. The work described in Chapter 3 was made possible through contributions from Simona Torriano (investigation, methodology, formal analysis), Abhishek Chadha (model development and validation), Sonia Barocio (investigation). Feedback and insight were provided throughout the duration of this work by Antonio Paniagua, Barry Burgess, Roni Hazim, and Nan Hultgren. Additional support included AAVS1 TALEN construct, which were provided by the Reza Ardehali Cardiology Research Lab at UCLA.

VITA

EDUCATION:

2016-2023 Ph.D. candidate in Medical and Molecular Pharmacology
University of California, Los Angeles, CA

2011-2013 M.S. in Biology, Specialization in Stem Cell Research
California Polytechnic University, San Luis Obispo, CA

2005-2010 B.S. in Biology
University of California, Los Angeles, CA

PUBLICATIONS:

Menon, T, AL Firth, DD Scripture-Adams, Z Galic, SJ Qualls, **WB Gilmore,** I Verma. (2015). Lymphoid Regeneration from Gene-Corrected SCID-X1 Subject-Derived iPSCs. *Cell Stem Cell*, *16*(4), 367–372. http://doi.org/10.1016/j.stem.2015.02.005

Lee, PC, B Truong, A Vega-Crespo, **WB Gilmore**, K Hermann, SA Angarita, et al. (2016). Restoring Ureagenesis in Hepatocytes by CRISPR/Cas9-mediated Genomic Addition to Arginase-deficient Induced Pluripotent Stem Cells. *Molecular Therapy - Nucleic Acids*, *5*(Supplement C), e394. http://doi.org/10.1038/mtna.2016.98

Ranjbarvaziri, S, S Park, NB Nguyen, **WB Gilmore**, P Zhao, & R Ardehali. (2017). Generation of Nkx2-5/CreER transgenic mice for inducible Cre expression in developing hearts. *Genesis (New York, N.Y. : 2000)*, *107*, e23041. http://doi.org/10.1002/dvg.23041

Mai, WX, L Gosa, VW Daniels, L Ta, JE Tsang, B Higgins, **WB Gilmore,** N Bayley, et al. (2017). Cytoplasmic p53 couples oncogene-driven glucose metabolism to apoptosis and is a therapeutic target in glioblastoma. *Nature Medicine*, *23*(11), 1342. http://doi.org/10.1038/nm.4418.

Pezhouman, A., JL Engel, NB Nguyen, RJP Skelton, **WB Gilmore,** R Qiao, D Sahoo, P Zhao, DA Elliott DA, R Ardehali. (2022). Isolation and characterization of human embryonic stem cell-derived heart field-specific cardiomyocytes unravels new insights into their transcriptional and electrophysiological profiles. *Cardiovasc Research*, 118(3):828-843. http://doi.org/10.1093/cvr/cvab102.

Gilmore, WB, NW Hultgren, A Chadha, SB Barocio, J Zhang, O Kutsyr, M Flores-Bellver, MV Canto-Soler, DS Williams. (2023). Expression of two major isoforms of MYO7A in the retina: Considerations for gene therapy of Usher syndrome type 1B. *Vision research*, *212*, 108311. https://doi.org/10.1016/j.visres.2023.108311.

Introduction

The Human Eye

The human eye is a spherical, liquid-filled organ roughly 2.5 centimeters in diameter and 8 grams in weight. The walls are composed of 3 tissue layers:

1. The external layer, consisting of the sclera and cornea, gives the eye its shape and strength. The sclera is a white fibrous tissue that provides structure to the organ. The cornea is a transparent part at the front of the eye where light is allowed to enter.
2. The intermediate layer consists of the iris, ciliary body, and choroid. The iris, the colored muscular part at the front of the eye, is responsible for controlling the amount of light entering the eye. The ciliary body surrounds the lens, helping focus incoming light and secreting aqueous humor. The choroid is a vascular tissue through which the majority of blood flows to and from the eye.
3. The inner layer lining the back of the eye is the retina. It is composed of neural and epithelial cells that function primarily to process incoming light into electrical signals, which then are sent to the brain in order to create the sense of vision. The vitreous humor, a translucent jelly-like substance, fills the core of the eye, and accounts for 80% of the eye's volume.

The Retina

The retina is an outermost extension of the central nervous system. During development, it arises from the optic vesicle before transforming into the optic cup and integrating into neighboring tissues that eventually comprise the eye. In adults, the retina is among the most metabolically active tissues in the human body. It is organized into eight structured layers:

1. Retinal Pigment Epithelium (RPE): Make up the external limiting layer between the choroid and neural retina layers. The RPE plays critical roles in maintaining photoreceptor health and overall homeostasis of the retina.
2. Outer limiting membrane (OLM): This region, also referred to as the photoreceptor outer layer (POL), consists primarily of photoreceptor outer segments containing dense stacks of discs filled with light sensitive biomolecules. These structures detect and initiate electrical impulses in response to activation from light.
3. Outer nuclear layer (ONL): Composed mostly of photoreceptor cell bodies, including a connecting cilium and a mitochondria-rich inner segment housing the cell nucleus.
4. Outer plexiform layer (OPL): Composed of synaptic terminations of photoreceptors connecting to bipolar cells.
5. Inner nuclear layer (INL): Made up of bipolar cell bodies transmitting signals to retinal ganglion cells. Lateral connections in this layer involve horizontal and amacrine cells.
6. Inner plexiform layer (IPL): Consists of synaptic connections of ganglion cell dendrites with bipolar cell and amacrine cell axons.
7. Ganglion cell layer (GCL): Contains the cell bodies of ganglion cells separated from each other by Müller cell processes.

8. Nerve fiber layer (NFL): Ganglion cell axons converge to form the optic nerve, through which signals are sent to the brain.

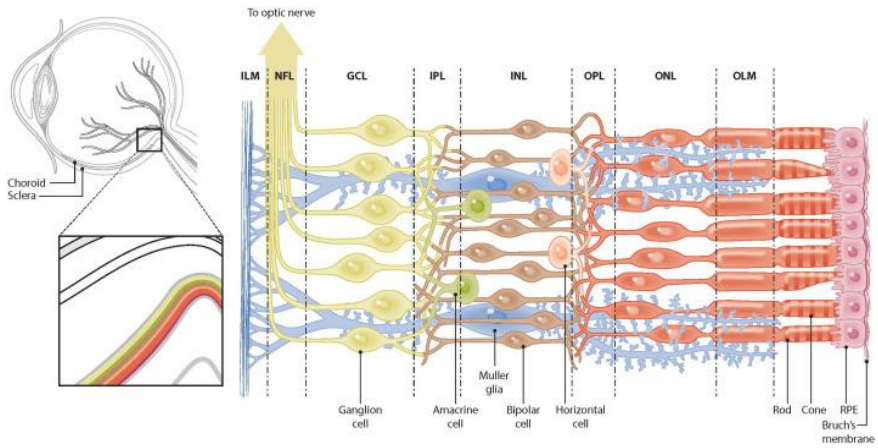

Figure A: 2D animation of retinal tissue layers, sectioned by dotted lines and labeled with bold abbreviations. Cell types are distinguished by color and noted with pointers. *Adapted from Kimbrel and Lanza, 2020.*

In the human retina, photoreceptor rods outnumber cones about 20 to 1, although this ratio varies from central to peripheral regions. Rods and cones are distinguishable from one another by distinct differences in disc organization. (Fig. B)

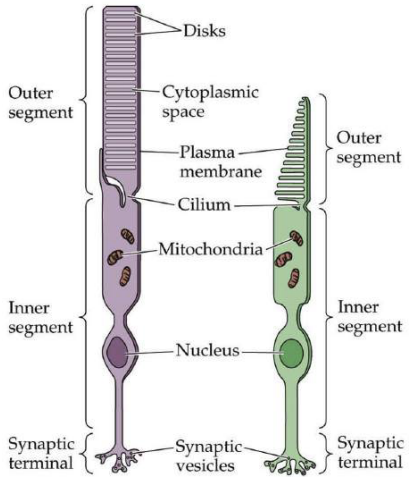

Figure B: Structural differences between rods (left) and cones (right).
Adapted from Purves et al., 2011.

A key anatomical region of interest for this dissertation spans from the rod and cone outer segments through the RPE. This includes the small gap interfacing photoreceptor outer segment (POS) tips and the apical RPE membrane, known as subretinal space. Interactions between the photoreceptor outer segments and RPE cells are a primary theme of this dissertation, and so understanding the general anatomy and biological activities operating in this region is paramount to understanding the following chapters.

The Retinal Pigment Epithelium

The RPE is a tightly packed polarized monolayer of pigmented cells comprising the outermost layer of the retina. As previously discussed, it is situated between the photoreceptors and the choroid, where it serves critical roles in maintaining homeostasis within the retina. RPE cells tightly interlock with one another, forming various junctions with neighboring cells. These include apical tight junctions and a basal cleft containing a variety of gap junctions, desmosomes, and adherens junctions. Tight junctions in the apical pole converge with retinal capillary endothelial cells to form the blood-retinal-barrier (BRB), an essential barrier that regulates molecules entering or leaving the retina. The basement of the RPE sits in contact with the Bruch's membrane, which separates the retina and the choroid. The basal region of the RPE houses the cell nucleus and major organelles, including the majority of mitochondria. The apical cell body contains a complex array of endosomes trafficking along cytoskeleton tracks, including phagocytosed POSs. Microvillar processes extend from the apical surface of the RPE into the subretinal space, where they ensheath adjacent photoreceptor outer segments. The resulting morphology of the RPE is a well-organized "cobblestone" tissue layer.

Functions of the RPE

Several functions of RPE have been characterized, including melanogenesis, phagocytosis, transepithelial transport, ion buffering, growth factor secretion, and visual cycle maintenance. These functions highlight the primary roles of the RPE – i) to establish a photoprotective and physical barrier between the eye and body, ii) to maintain photoreceptor

health and function, and iii) to establish and maintain a sensitive environment in the retina. To better understand the later chapters, this section is dedicated to discussing some of these functions in further detail.

1. Melanogenesis and photoprotection

A distinguishing characteristic of RPE cells is their dark coloration, resulting from the manufacturing of melanin-filled organelles called melanosomes. These serve primarily as a photoprotective shield by absorbing light that passes through the photoreceptor layer. Any focused or scattered light that passes through photoreceptors can harm exposed tissues through photo oxidation. Melanosomes absorb and filter this light radiation, helping reduce exposure and photodamage to underlying RPE organelles and neighbor cells. Various melanin pigment molecules (eumelanin, pheomelanin, and neuromelanin) are synthesized and stored by melanosomes, each possessing a distinct spectrum of light absorption. Altogether, these melanin compounds provide melanosomes their broad-spectrum absorption capacity for visible light and UV radiation. Absence of pigmentation in the RPE from albinism results in visual symptoms, such as increased light sensitivity (photophobia) and underdeveloped fovea. (McKay, 2019)

Melanosome formation in the RPE follows similar stages as in melanocytes. Unlike melanocytes, however, RPE cells retain their melanosomes primarily formed during embryonic development. (Storm et al., 2020) Also, RPE melanosomes are uniquely capable of navigating to the apical processes of the cell. Such trafficking requires i) dynein-dependent motility to the apical cell body, and ii) the transfer from microtubules in the cell body onto actin filaments

extending up into the apical processes. (Jiang et al., 2015) Expression of an actin motor (myosin VIIa), an adapter (MyRIP), and a GTPase (Rab27a) are required for this transfer and subsequent travel of melanosomes within the apical processes. (El-Amraoui et al., 2002; Futter et al., 2004; Gibbs et al., 2004; Lopes et al., 2007) In some organisms, this translocation is light-induced. (Zhang et al., 2013) Distribution and morphology of melanosomes within the cell provide some indication of healthy RPE function, as some genetic mutations result in abnormalities. (Storm et al., 2020)

2. Phagocytosis

Throughout one's lifetime, RPE cells phagocytose the most cellular material of any cell in the body, primarily from photoreceptor cell outer segments. (Mazzoni et al., 2014) Photoreceptor cells continuously renew discs, thereby extending their outer segments. As these discs mature, they continuously grow outward, accumulating damage as they age from processing incoming light. Photo-oxidation leads to accumulation of damaged proteins, lipids, and reactive oxygen species (ROS) at the photoreceptor tip, which then must be ingested and processed through close collaboration with the RPE. Specific receptors along the surface of the RPE aid in recognition and adhesion to outer segment tips, which activate signals that initiate phagocytosis. During this process, the distalmost segments of photoreceptors are engulfed and digested by RPE cells. (Young, 1967; Young and Bok, 1969) In order for the RPE to keep up with the rate of disc synthesis (about 10% of the POS each day), (Young and Bok, 1969) prompt cytoskeletal rearrangement along the apical surface is required. Circadian cycling helps synchronize RPE phagocytic processes with the rhythm of the photoreceptor of outer segment

renewal. (Goldman et al., 1980; LaVail, 1980) Considering that in humans, each RPE cell supports roughly 20 photoreceptors, close collaboration between these cells is critical for maintaining order in this metabolically demanding process.

The molecular mechanism of RPE phagocytosis involves a series of stages. Receptor-mediated endocytosis involves an array of interactions between "ready-to-eat" POSs and apical RPE membrane proteins, some of which have been identified and characterized. Phosphatidylserine (PS) externalized to the outer POS membrane serves as the primary 'eat me' signal for RPE. Protein adapters secreted into the subretinal space cap PS residues, facilitating binding to receptors on the RPE. Binding of milk fat globule-EGF factor 8 protein (MFG-F8) to αvβ5 on the RPE activates focal adhesion kinase (FAK), a downstream regulator of MerTK. MerTK plays a critical role in initiating F-actin polymerization and branching, driving the engulfment of outer segments tips. Protein S and Gas6 binding to MerTK initiates this process. Knockout studies in rodent models demonstrate impaired or complete absence of POS engulfment in the absence of MerTK or its ligands. (Feng et al., 2002; Mullen and LaVail, 1976; Burstyn-Cohen et al., 2012) Similarly, knockout of αvβ5 or its ligand significantly impairs the rate of POS ingestion, while also decoupling the process from its natural diurnal rhythm. (Nandrot et al., 2004; Nandrot et al., 2007)

Ingested POSs, now phagosomes, are trafficked from apical to basal regions of the cell, undergoing sequential fusion to endosomes and lysosomes as they mature. Essential compounds, such as 11-*cis* retinal and docosahexaenoic acid (DHA), (Gordon et al., 1992; Thomson and Gal, 2003) must be separated from waste and recycled back to photoreceptors. The remaining waste must be broken down by lysosomes and deposited into the bloodstream

via the choroid. Impairments to phagosome trafficking has been shown in cells lacking myosin VIIa, resulting in the buildup of apically localized phagosomes in the RPE. Multiple Rab proteins have been implicated in regulation of endosome, phagosome, and lysosome interactions, though much of the mechanisms involved are poorly characterized. Autophagic trafficking has also been suggested to mediate some phagosome trafficking, further demonstrating the complexity of RPE intracellular processing.

3. Other functions of the RPE

Maintenance of the visual cycle is another essential role of the RPE that relies on POS phagocytosis and intracellular trafficking. The chromophore 11 cis-retinal is an essential component of light sensitivity by photoreceptors, binding to rhodopsin to facilitate phototransduction reactions. (Beahr, et al., 2003) Due to insufficiencies of photoreceptors in producing this visual cycle intermediate, RPE must biochemically convert all-trans retinol to 11 cis-retinal, which is then recycled back to photoreceptors through the subretinal space.

The RPE also helps maintain the architecture of the surrounding matrix and vasculature through the secretion of growth factors. Basolateral secretion of the vascular endothelial growth factor (VEGF) and apical secretion of pigment epithelial derived factor (PEDF) help maintain the sensitive vascular architecture of the retina and that of the neighboring choriocapillaris. (Blaauwgeers et al., 1999) VEGF production stabilizes fenestrations along the choriocapillaris endothelium, which in turn allows vital nutrients, including vitamin A, to permeate through to the RPE. (Roberts et al., 1995) Further support for endothelial cells and the surrounding extracellular matrix (ECM) comes from matrix metalloprotease (TIMP)

secretion. (Padgett et al., 1997) The RPE also secretes neuroprotective factors to protect photoreceptors in response to injury, including basic fibroblast growth factor (bFGF) and ciliary neurotrophic factor (CNTF). (Cao et al., 1997) Together, these factors and others help support and maintain a healthy environment within and around the retina.

A well-established barrier allows the RPE to strictly manage the flow of nutrients, waste, and ions entering or exiting the retina. The electrochemical activity of photoreceptors demands stable pH and ion concentrations in the inner retina. The RPE helps to mitigate these fluctuations in environmental conditions, largely through transepithelial transport of water and ions through transmembrane pumps.

As a result of such close functional collaboration between the RPE and photoreceptors, they are often considered as a single functional unit. Impairment to either or both RPE and photoreceptors due to genetic mutations results in inherited retinal disease.

Inherited Retinal Diseases

Inherited retinal dystrophies (IRD) are a group of clinically heterogeneous and genetically diverse diseases that result in progressive vision loss. They affect approximately 1 in 3,500 individuals and are caused from transmission of genetic mutations in disease-causing genes involved in healthy retina function, over 270 of which have been identified. (Henderson, 2020) Clinical symptoms include impairments to night vision, visual acuity, color distinction, and visual field. Depending on the disease, symptoms can present from birth up through middle age. Certain allelic variations can predispose individuals to age-related retinal disease, such as age-related macular degeneration (AMD), though such variations should not be confused with disease-causing genes.

IRDs can be categorized based on the subtype of cell predominantly affected, such as cone, rod-cone, macula, etc. Dystrophies involving the macula, such as Stargardt disease, present as loss of central vision, impaired color and contrast sensitivity, and photophobia. For many pigmentary retinopathies, where the periphery of the retina is predominantly affected, retinitis pigmentosa (RP) presents as a clinical hallmark of retinal degeneration. Photoreceptor and RPE cell death cause lesions in the retina that are distinguishable by deposits of pigment and cell debris. As disease progresses, RP lesions expand outward, progressively depleting the visual field, ultimately resulting in blindness. Most known IRDs are caused by mutant genes expressed by photoreceptors, however a subset of these genes is expressed in both RPE and photoreceptor cells. *MYO7A* is one such gene which expresses predominantly in RPE cells.

The most optimal clinical outcome relies on early disease detection, especially for IRDs involving irreversible tissue degeneration. For diseases presenting in early life, the therapeutic

window for patients to receive treatment is limited. Early clues of retinal disease include nystagmus, visual loss, photophobia, and, in the case of deaf-blindness diseases, hearing and balance issues. (Suppiej, et al., 2019; Prokofyeva et al., 2011) Lifestyle changes may help mitigate some forms of retinal disease, especially those affecting nutrient metabolism, though this may be limited to subjects predisposed to AMD or diabetic retinopathy. Retinal imaging can be used to objectively diagnose and assess degree of damage in suspected cases. (Georgiou et al., 2020) Clear disease diagnosis can be accomplished through genetic testing, though these methods have not been widely adopted into public health systems for a number of reasons.

Understanding one's genetic background is the best predictor of clinical pathology, and developing treatment plans for a number of genetic diseases. Clinical studies have demonstrated that different mutant alleles of the same gene can produce different severity of disease. A growing understanding of the genetic basis underlying disease has paved the way for gene therapy.

Treatments for IRDs

Currently, definitive treatment options for IRDs are extremely limited. Molecular profiling of patients is a fundamental step for facilitating access to advancing therapy options. Once degeneration takes place in the retina, restoring function to the damaged areas is currently not feasible. Significant efforts over the past two decades have been directed towards developing effective IRD treatments, focusing on innovative therapies aimed at halting disease progression and reversing vision loss altogether. At present, there are roughly 130 therapeutic

agents in various stages of clinical investigation. (Cross et al., 2022) These strategies are broadly characterized into gene-dependent and gene-independent approaches.

Gene-independent approaches

These treatment approaches are not tied to a particular genetic mutation, making them potentially beneficial to a variety of IRDs. Though no therapies in this category are currently available, pre-clinical research and trials are currently underway that could, in principle, provide therapeutic benefit.

Cell replacement therapy aims to regenerate or replace diseased tissues through the introduction of donor tissue. These donor tissues are typically derived from progenitor stem cells. These pluripotent cells can be expanded and then differentiated into the wide variety of cell types and tissues that comprise the body. Once differentiated to their desired state, these cells can then be transplanted to the site of disease in the hope of alleviating disease symptoms. Such an approach requires the integration and survival of donor neural retina (NR) and retinal pigment epithelium (RPE) tissues to replace what has been damaged. Cellular transplantation of RPE may be more amenable than NR tissues, since this tissue does not require intricate synaptic connection to neighboring cells in order to function. This approach has been explored in a small patient cohort. (Mandai et al., 2017; Schwartz et al., 2014) Currently active clinical trials are underway exploring this method. (da Cruz et al., 2018) Other cell therapy trials involve an intravitreal injection of allogeneic retina progenitor cells (jCyte, ClinicalTrials.gov ID: NCT03073733; ReN-003, ClinicalTrials.gov ID: NCT02464436).

Gene-dependent approaches

Genetic characterization of diseased subjects determines what forms of treatment are feasible. Gene-based approaches involve either manipulation of DNA based on the affected mutant gene or intervention at the RNA level.

Antisense Oligonucleotides

A significant portion of IRDs is caused by either mutations in splice sites or intronic regulatory elements. One potential approach for treating such cases involves the use of antisense oligonucleotides (AONs). These short, synthetic oligodeoxynucleotides are designed to target and alter specific RNA sequences through complementary binding, resulting in modified protein expression. In the case of aberrant splicing, the aim is to eliminate or correct expression of disease-causing gene variants. This can be accomplished through exon skipping or endonuclease mediated knockdown, depending on the AON complementary to designated RNA sequences.

Treatment of IRD models with AONs has been demonstrated in some preclinical studies to correct for mutations in large genes. Nearly complete elimination of a disease-causing pseudo exon in cells containing the most recurrent CEP290 gene mutation demonstrated therapeutic potential for one form of Leber congenital amaurosis (LCA). (Collin et al., 2012; Gerard et al., 2012) More recently, a similar approach was used to correct splicing due to an intronic mutation in USH2A patient-derived fibroblasts. (Slijkerman et al., 2016) Treatment with AONs in a humanized mouse model of Usher Syndrome 1C was shown to partially rescue hearing loss caused from aberrant splicing of the USH1C gene. (Lentz et al., 2013) A major

limitation of these and other gene therapies is effective delivery to diseased tissue, especially for the sensitive tissues of the retina, though delivery vectors continue to improve, as is discussed below.

Approximately 11% of all inherited diseases and 12% of IRDs are due to premature termination codons (PTC) caused by nonsense mutations. (Mort et al., 2008; Samanta et al., 2019) The broad patient population carrying these mutations makes translational read-though inducing drugs (TRIDs) an intriguing therapeutic option, since a single drug could theoretically be used to treat a wide range of diseases. In essence, these drugs by causing ribosomes to skip over stop codons, resulting in the translation of a full-length protein instead of the default truncated form. For this to be therapeutically effective, a drug must selectively target PTCs with minimal to no effect on regular stop codons. Aminoglycosides, a class of antibiotics, have been shown to preferentially target PTCs and induce read-through, though investigation into the use of these compounds has been largely abandoned due to toxicity issues. Their promise has, however, inspired the exploration of new PTC-suppressing drugs, several of which have been identified and explored for treating IRDs. (Moosajee et al., 2008; Goldman et al., 2012; Cunha et al., 2023) Ongoing clinical research using TRIDs to treat IRDs caused by nonsense mutations demonstrates the ongoing interest and potential of this therapeutic approach.

Gene Therapy

Gene therapy is a promising approach for treating genetic disease. Conceptually, it is a simple idea - introduce a piece of genetic material to a targeted cell or tissue type that will result in reversal or deceleration in the progression of a disease. For this to make sense as a therapy, many factors need to be carefully considered. With regards to the diseased cell being treated, expression of introduced genetic material needs to be stable, sustained, and properly regulated. This would require either DNA integration of the into the host cell or episomal maintenance of genetic material. Integrating vectors must be considered carefully in order to avoid the potentially genotoxic effects of insertional mutagenesis, making site-specific integration an attractive approach to gene therapy. Episomal maintenance does not rely on DNA integration, and is therefore considered by many to be a safer approach for gene delivery to cells. With regards to the system surrounding the treated cells, delivery of genetic material should cause minimal to no adverse or undesirable response, such as immune reaction or injury. Therefore, choosing the appropriate approach and delivery vector for each gene therapy is a delicate decision.

General Design

The first considerations for designing a gene therapy are designing, assembling, and testing potentially therapeutic gene vectors in an appropriate disease model. Generally, a DNA vector construct is initially assembled, which includes a few essential elements: i) a promoter, ii) a coding gene or genes, and iii) a termination signal. The specific components that comprise each element and the overall construct size depend on the desired gene therapy. Additional

elements can be added in order to improve vector function, meet specialized requirements, or to facilitate packaging into a delivery vector. Many elements are re-engineered into miniaturized forms in order to comply with size restrictions, especially when packaging into viral vectors. A viral vector's genetic cargo refers to the number of nucleotides that spans the distance between terminal repeats – ITRs for AAVs and LTRs for lentiviruses. For a construct to fit into a single delivery vector particle, the total genetic composition must be smaller than the viral cargo capacity. Further details involving delivery vectors will be discussed later.

Once a suitable vector construct is assembled and, if necessary, packaged into a delivery vector, a series of experiments are generally performed to test for functionality in a disease model. Common indicators of a working vector construct include sustained, stable gene expression and functional rescue of disease phenotypes. Once validated, and proof-of-concept is firmly established, the choice on whether to proceed into clinical translation studies can then be considered.

General Approaches

The classic approach to gene therapy is gene augmentation, which involves delivery of a full-length cDNA of a healthy gene to diseased tissues. The first clinical attempts at such an approach were led by French Anderson, and focused on genetic diseases of the blood and immune system. (Anderson et al., 1990) Their first success came from using recombinant retroviruses to establish healthy adenosine deaminase (ADA) expression in ADA-deficient SCID patients. (Kohn et al., 1989) In this case, the therapy was administered ex vivo - cells were extracted and treated with the gene therapy, and then reinfused back into the patient. Gene

augmentation therapy can also be delivered directly in vivo through injection at or nearby the site of disease. Though promising, the gene augmentation approach does have some major limitations. Firstly, it relies on the stable delivery and long-term expression of exogenous "healthy" DNA to diseased cells, a process that could disrupt the endogenous genetic environment if improperly integrated into the genome. Also, only a single isoform of the augmented gene is generally considered, which, in some instances, could be insufficient for disease rescue.

The alternative to gene augmentation is genetic repair. With this approach, the specific disease-causing mutations are corrected within the endogenous genes of the diseased cell. Genetic repair can be accomplished through different mechanisms, including homology-directed repair (HDR) or base editing. Pioneering work for HDR from the 1980's demonstrated that exogenous DNA could be integrated at defined chromosomal regions by homologous recombination (HR). (Smithies et al., 1984, 1985) Generating a double-stranded break (DSB) in the DNA at the site of insertion greatly improves the efficiency of recombination. (Kucherlapati at al., 1984; Smithies et al., 1985) Targeting DSBs to precise regions of the genome can be accomplished using customizable, site-specific nucleases, such as zinc-finger nucleases (ZFNs) (Kim et al., 1996; Urnov et al., 2010), transcription activator-like effector nucleases (TALENs) (Christian et al., 2012; rev Bogdanov et al., 2011), and more recently, CRISPR-associated nucleases, such as Cas9. (Cong et al., 2013; Mali et al., 2013). ZFNs and TALENs are bulky heterodimeric proteins consisting of a DNA-binding domain fused to a Fok1 endonuclease, and must be individually constructed for each genetic target. Cas9 consists of a single protein with

two functional nuclease domains (RuvC and HNH), which are directed by an easily programmable guide RNA molecule.

When expressed, programmed nucleases scan the genome for their target sequences and generate cuts at specific loci. In the result of a DSB, the DNA must be repaired by either non-homologous end joining (NHEJ) or homologous recombination (HR). The default cellular DNA repair pathway is non-homologous end joining (NHEJ), in which each end of the DSB is ligated together, often resulting in the formation of indels (nucleotide insertions or deletions) at the site of repair. If multiple DSBs are generated in the same region, complete excision of the material between the breaks can occur. Either excision or indel formation usually causes disruption of the targeted gene, resulting in a functional knockout of the target gene. Alternatively, when a repair "donor vector" template is presented during repair, homologous recombination can occur, driven by regions of homology between the endogenous DNA and the donor vector. Clonal expansion of HDR-edited cells is a popular approach for isolating cell populations relevant for therapeutic application or research purposes. This approach was used to generate a disease model cell line in Chapter 3 of this dissertation. Gene augmentation or editing for therapy could be accomplished using HDR, however, this approach is less practical than other options, mostly due to poor recombination efficiencies, especially with large inserts.

A more recently discovered approach to gene therapy involves repair of harmful mutations without the requirement of DSBs. This has been made possible through advancements in CRISPR/Cas technology. Cas9 derived from *Streptococcus pyogenes* was the first CRISPR tool adapted for mammalian gene editing. (Jinek et al., 2012) Since then, the CRISPR/Cas system has been reengineered into a large suite of genetic tools capable of

performing a multitude of functions. Early versions, such as the Cas9 nickase (Nishimasu et al., 2014) and dCas9 (Qi et al, 2013), had modified nuclease domains that enabled functions beyond just DNA cutting. Fusion of additional motifs to these versions further expanded the capabilities of the CRISPR/Cas system, enabling functions such as gene activation, (Chen et al, 2017), epigenetic modification, (Chen et al 2022), improved HDR efficiency (Park et al, 2021), and precision base editing. (Komor et al 2016; Gaudelli et al 2017) Although no therapies using these technologies are currently available, many trials continue to advance through preclinical and clinical pipelines. This is the primary topic of Chapter 3 of this dissertation.

Delivery Approaches

Once a therapeutic approach decided and tested, the next consideration is the delivery method. Therapeutic vectors developed to overcome the obstacles of gene delivery are broadly classified into 2 types: non-viral and viral. Non-viral vectors include naked DNA or RNA, liposomes, nanoparticles, and other means. Naked DNA was the first vector ever used to successfully deliver recombinant DNA into mammalian cells with therapeutic implication in mind. (Cline et al.,1980; Friendmann 1992) In these pioneering studies led by Martin Cline, human globin gene was introduced into murine bone marrow cells by calcium phosphate transfection. (Friendmann 1992) Though feasible to deliver genetic material by this approach, clinical application has been limited by low delivery efficiency and safety concerns. (Tsurumi et al., 1996) Because of this, the use of non-viral vectors for gene therapy has been largely overlooked. Recently, however, advancements in nanoparticle technology have broadened the scope of non-viral vectors for gene therapy. Nanoparticle vectors typically consist of some

therapeutic material, such as a functional gene cassette, encased in biocompatible material engineered to target a specific cell type. These vectors can be produced consistently in large amounts and have minimal toxicity or immunogenicity. The particle size and outer coat can be customized to control delivery and biodistribution (Mitchell et al., 2021). Unlike viral vectors, the manufacturing of nanoparticle vectors does not require a biological host, meaning production is far less complicated and much more cost effective. Despite early skepticism of gene transfer efficiency and target specificity, nanoparticle vectors could provide solutions to the shortcomings of viral vectors, and could very well be a cornerstone for the future of gene therapy.

Over the past half century of gene therapy research, viral vectors have been the most popular approach for gene transfer. Viruses have evolved alongside the animals for millennia, finding different cellular pathways to exploit in order to gain access to cellular niches that support their own reproduction and persistence. The ability of certain viruses to genetically reprogram cells upon infection inspired the idea of transforming these pathogens into medicine. For gene therapy, ideal viral vectors mimic this infection process but avoid viral gene expression that causes replication and toxicity. This is done by removing some or all viral coding regions, preserving essential sequences for functions like packaging and integration into host DNA. The desired therapeutic gene is then inserted into this modified backbone to generate a complete viral vector construct. The viral vector particles are produced in packaging cells, and then purified and quantified in preparation for testing or patient delivery.

A variety of viral vectors are commonly used for gene transfer, the main ones being herpes simplex virus-1 (HSV-1), lentivirus, adenovirus, and adeno-associated virus (AAV).

(Thomas et al, 2003) Each vector has its own advantages and disadvantages, all of which must be considered when designing a therapy for a specific disease. (Fig. D) Viral particles consist of genetic material encased in a capsid, with some classes of viruses containing an outer envelope. Retroviral-mediated gene transfer was the first approach proposed in the early 1980's. (Shimotohno, 1981; Wei, 1981) The ability of this approach to complement genetic defects and correct disease phenotypes was demonstrated shortly thereafter. (Jolly, 1983; Miller, 1983; Willis, 1984) The potential oncogenic effect of integrating viruses was demonstrated around the same time, (Tabin, 1982) bringing forth safety concerns and raising caution for clinical translation into humans. Adenovirus was the first viral vector developed for clinical trials of gene therapy in 1990. (Goswami et al., 2019) The dangers of viral-mediated immune reactions were made clear following the tragic death of a patient administered an adenovirus in a gene therapy clinical trial for ornithine transcarbamylase deficiency in September 1999. Since then, AAV and lentiviral vectors have become the favored systems for gene transfer, as they both produce sustained gene expression in a wide variety of cell types, without relatively low risk for causing inflammation.

Vector	Genetic material	Packaging capacity	Tropism	Inflammatory potential	Vector genome forms	Main limitations	Main advantages
Enveloped							
Retrovirus	RNA	8 kb	Dividing cells only	Low	Integrated	Only transduces dividing cells; integration might induce oncogenesis in some applications	Persistent gene transfer in dividing cells
Lentivirus	RNA	8 kb	Broad	Low	Integrated	Integration might induce oncogenesis in some applications	Persistent gene transfer in most tissues
HSV-1	dsDNA	40 kb* 150 kb‡	Strong for neurons	High	Episomal	Inflammatory; transient transgene expression in cells other than neurons	Large packaging capacity; strong tropism for neurons
Non-enveloped							
AAV	ssDNA	<5 kb	Broad, with the possible exception of haematopoietic cells	Low	Episomal (>90%) Integrated (<10%)	Small packaging capacity	Non-inflammatory; non-pathogenic
Adenovirus	dsDNA	8 kb* 30 kb§	Broad	High	Episomal	Capsid mediates a potent inflammatory response	Extremely efficient transduction of most tissues

*Replication defective. ‡Amplicon. §Helper dependent. AAV, adeno-associated viral vector; dsDNA, double-stranded DNA; HSV-1, herpes simplex virus-1; ssDNA, single-stranded DNA.

Figure C: Table outlining critical properties of popular viral vectors used in considering approach for therapeutic gene transfer.
Adapted from Thomas et al., 2003.

Gene Therapy in the Retina

Gene therapy has emerged as a promising approach for treating previously incurable genetic diseases of the retina. Pioneering studies by Jean Bennett led the first demonstration of successful gene delivery to an animal retina using an adenovirus vector. (Bennet et al, 1996) Further development of this work led to the first ever FDA approval for the retinal gene therapy Luxturna, an AAV-based delivery of *RPE65* cDNA for the treatment of Leber congenital amaurosis (LCA), in December 2017. Following the success of these studies, there has been a surge in the research and development of retinal gene therapies. AAV delivery of *PRPH2* cDNA marked the first demonstration of gene therapy correcting both morphological and functional defects of the retina. (Ali et al., 2000) Retinitis pigmentosa (RP) is the most common hereditary retinal and is theoretically treatable using gene therapy. Current retinal gene therapies, such as

vMCO-010, GS-030, and AGN-151597, are leading the charge in meeting currently unmet clinical needs for RP treatment. (Cross et al., 2022) Additional hurdles still remain for treating certain disease-causing mutations in scenarios where gene augmentation may not be an appropriate approach. These topics are the focus of Chapters 1 and 3 of this dissertation.

Chapter 1: *MYO7A* Isoforms

Retinal degenerations (RDs) due to monogenic mutations occur at a frequency of approximately 1 in 2000, worldwide. (Berger et al., 2010) Most of these degenerations (70% according to RetNet) are recessively inherited, caused by loss of gene function, so that the disease can potentially be treated by the introduction of a normal (WT) copy of the mutant gene. Such gene augmentation therapies have now been attempted for numerous genes, with one FDA-approved product so far; in 2017, approval was given for treating a form of Leber congenital amaurosis (LCA2), which is caused by biallelic mutations in *RPE65*, by delivering WT *RPE65* to the RPE with adeno-associated virus (AAV). (Russell et al., 2017) Similar approaches for several other inherited RDs are in clinical trials. (Rakoczy et al., 2019, Cehajic-Kapetanovic et al., 2020, Fischer et al., 2020, Yu-Wai-Man et al., 2020)

A limitation of gene therapy, whether by augmentation or in situ editing of the mutation, is that the retinal cells need to be treated before there is too much degeneration, as it is dependent on the presence of healthy cells to start expressing the introduced WT copy of the gene. In LCA2 cases, administration of treatment in older patients has been found to be less efficacious in the long term. (Cideciyan et al., 2013) This limitation means that patients should be identified before manifestation of retinal disease. LCA2 patients are born blind due to disruption of the visual cycle, so that young patients can be potentially identified before the onset of RD. However, for many other inherited RDs, pending blindness is only noticed once there is loss of peripheral vision, which may not occur until a significant portion of photoreceptor cells have degenerated or at least have been damaged.

Usher syndrome (USH) is a deaf-blindness disorder, caused by recessive mutations in any one of numerous autosomal genes, nine of which have been identified and confirmed. (Williams, 2008, Castiglione & Moller, 2022) The deafness precedes RD and is most obvious in USH1 patients, who are born profoundly deaf. Most of these patients are now treated with cochlear implants to address their deafness. The early identification of these patients, before the onset of RD, means that USH patients represent a highly suitable population for retinal gene therapy.

Commonly, gene augmentation approaches involve the delivery of a single cDNA sequence of the WT gene. Despite the successes of this approach, it is potentially limited in cases where the mutant gene normally expresses more than one isoform. Previously, we noted that most of the USH genes might express more than one isoform. (Williams et al., 2017)

Here, we focused on retinal isoform expression of the most common USH1 gene, *MYO7A*, which underlies USH1B (Weil et al., 1995). *MYO7A* encodes the heavy chain of an actin-based motor protein. (Udovichenko et al., 2002) Our results show that the neural retina and RPE from human, pig, and mouse all express two isoforms of *MYO7A*. We discuss the relevance of our findings to USH1B gene therapy approaches.

2. Materials and methods

2.1. Human and animal tissues

C57BL6 mice carrying WT *Myo7a* on both alleles were maintained as described (Gibbs et al., 2003). Young mice, aged postnatal day 9–15, were used due to the relative ease of separation of RPE from neural retina (NR). Mouse NR samples were comprised of pooled tissues

from each eye to ensure sufficient RNA yields. To obtain sufficient material for analysis, mouse RPE was cultured and expanded for 3–5 days. These primary mouse RPE samples were combined when harvesting RNA. Pig eyes were obtained through UCLA Division of Laboratory Animal Medicine (DLAM). Eyes were excised from the eye socket and dissected to expose the tissues of the retina. The neural retina was separated from the eyecup and set aside for further processing. The RPE layer was carefully isolated from the eyecup by mechanical separation. De-identified samples of post-mortem posterior eye segments (from a 42-year-old male and a 90-year-old female, neither with any known retinal disease) were provided by the laboratory of Dr Gabriel Travis, at the Stein Eye Institute, according to regulations for anonymous pathological specimens. All tissue samples were immediately processed following isolation, or otherwise flash frozen and stored at -80°C.

2.2. Cell culture

ARPE-19 cells were thawed and cultured in DMEM/F12 with GlutaMAX, 10% FBS, 100 U/mL Penicillin and 100 U/mL Streptomycin, until confluency was reached. Cells were then passaged and seeded into a new culture plate (1.66×10^5 cells/cm^2) with differentiation medium (MEM-Nic with GlutaMAX, 1% FBS, 100 U/mL Penicillin, 100 U/mL Streptomycin, 1% N1 supplement, 0.1 mM NEAA, taurine (0.25 mg/ml), hydrocortisone (20 ng/ml), triiodo-thyronine (0.013 ng/ml), and 10 mM nicotinamide). (Hazim et al., 2019, Hazim et al., 2022) The cells were maintained for at least 14 days at 37 ◦C, 5% CO2 with media changes every 2–3 days until a polarized morphology was established.

The H9 embryonic stem cell line used in these studies was generated by WiCell (Madison, Wisconsin), and provided for our studies through the UCLA Broad Stem Cell Research

Center Stem Cell Bank. The xcHUF1 iPS cell line was also obtained through the UCLA Stem Cell Bank facility, where the line was generated by lentiviral cassette integration of the reprogramming factors Oct4, Sox2, Klf4, and cMyc. This line originated from an individual with no known retinal disease, and was used only for isolated iPSC-RPE cultures.

All stem cells were plated and maintained on Matrigel® Basement Matrix-coated tissue culture plates and cultured in mTeSRTM1 Basal Medium. Differentiation from pluripotent state into RPE was performed using a described 14-day differentiation protocol (Buchholz et al., 2013) with modifications. (Hazim et al., 2017) Briefly, plated ESC or iPSC colonies were cultured for days 0 and 1 in basal medium supplemented with Noggin (50 ng/mL), Dkk1 (10 mg/mL), and IGF1 (10 mg/mL). On day 2, the culture media is replaced with basal medium supplemented with Noggin (10 ng/mL), Dkk1 (10 mg/mL), and IGF1 (10 mg/mL), and bFGF (5 ng/mL). On day 4, the medium is again replaced, this time with basal medium supplemented with Dkk1 (10 ng/mL) and IGF1 (10 ng/ mL). For days 4 through 14, differentiating cultures were maintained in fresh basal medium supplemented with Activin A (100 ng/mL) and SU5402 (10 µM). Finally, after 14 days, culture media is switched to MEM-Nic with 5% FBS, and replaced every 2–3 days until pigmented, cuboidal RPE cells begin to appear within the culture. These patches of RPE were mechanically isolated, and expanded into homogenous hiPS-RPE or hES-RPE cultures. Retinal organoids were generated from an hiPSC line derived from CD34+cord blood (A18945, Thermo Fisher Scientific). (Burridge et al., 2011) The karyotype of this cell line was verified to be normal. Undifferentiated hiPSCs and derived retinal organoids were routinely tested to confirm the absence of contamination by mycoplasma (PCR Universal Mycoplasma Kit, ATCC), bacteria and fungi. Cell culture, retinal differentiation, and organoid formation were conducted as

described previously. (Zhong et al., 2014, Aparicio-Domingo et al., 2023) Retinal organoids at 270 days of differentiation were used for these studies. Induced primary RPE were obtained from retinal organoids (ro-RPE), as described. (Flores-Bellver et al., 2021) Briefly, RPE tissue was isolated from retinal organoids at 60 days of differentiation, and then enzymatically dissociated into single cells, and seeded on to Transwell culture membrane inserts (No. 3460, Corning), coated with Matrigel matrix (No. 354230, Corning). RPE cells were maintained at 37°C and 5% CO2 in MEM-Nic as described above but with 5% FBS, as described previously (Maminishkis et al., 2006), until they were fully differentiated.

2.3. Isoform-specific full length cDNA construct cloning and sequencing analysis

Full length *MYO7A* or *Myo7a* was PCR amplified from RPE samples using the following primers:

hMYO7A Forward:	5'-ATGGTGATTCTTCAGCAGGGG-3'
hMYO7A Reverse:	5'-TCACTTGCCGCTCCTGGA-3'
mMyo7a Forward:	5'-ATGGTTATTCTGCAGAAGGGGG-3'
mMyo7a Reverse:	5'-TCACCTTCCACTCCTGGAGT-3'
pMyo7a Forward:	5'-ATGGTGATTCTTCAGCAGGGG-3'
pMyo7a Reverse:	5'-TCACTTGCCACTCCTGGAG-3'

The resulting amplicons were submitted for Sanger sequencing (Laragen, Culver City, CA), using the sequencing primer IFID Forward (5'-AAGGGGATTTATGCCCAGAG-3'). The resulting chromatograms were viewed using SnapGene software (San Diego, CA). Human and mouse *Myo7a* PCR products were cloned into TOPO backbone plasmid using the TOPO TA Cloning kit (ThermoFisher), transformed into competent bacteria, and plated onto LB agar plates supplemented with Kanamycin (50 μg/mL). Clonal transformants were grown up in LB +

Kanamycin cultures. Plasmid DNA was purified by Purelink Quick Plasmid Miniprep Kit (Invitrogen). Purified plasmid DNA was submitted for Sanger sequencing (Laragen, Culver City, CA).

2.4. Sample preparation for quantitative PCR

The expression of *MYO7A* or *Myo7a* in collected samples was verified using quantitative reverse transcription-PCR (qRT-PCR). Total RNA was extracted from samples using the RNeasy Mini Kit (Qiagen), as described by the manufacturer's protocol. Fully polarized ARPE-19 cells were washed twice with PBS prior to harvest, and then mechanically scraped from the culture well for RNA extraction. Samples of RPE from retinal organoids (ro-RPE) were incubated in RNA Protect (Qiagen, Hilden, Germany) to attenuate endogenous RNase activity and mRNA synthesis, and then scraped off the plate into a 1.5-ml tube. Cells were centrifuged at 2500*g* for 10 min and the pellet was resuspended in buffer RLT plus (RNeasy Plus Micro/Mini Kits; Qiagen) with 2-mercaptoethanol (1:100; Sigma–Aldrich Corp.). In the case of retinal organoids, neural retina devoid of RPE was used. Retinal organoid samples were washed twice with PBS and then incubated with 150 µL of TRIzol reagent (Thermo Fisher Scientific, USA) for 5 min. at room temperature (RT). The mixture was vortexed well to ensure complete lysis of the tissue. This was followed by the addition of 30 µL of chloroform (Sigma Aldrich, USA), vigorously shaken, and incubated for 3 min at RT. Samples were then centrifuged for 5 min at 12000*g* at 4°C to separate the phases. The aqueous phase was collected carefully, so not to disturb the interphase, and dispensed into another microtube for further RNA processing. Primary mouse and pig tissues were collected and homogenized, then passaged through a syringe to facilitate

dissociation. Purified RNA was eluted from the column with a maximum of 40 µL Ultrapure RNase-free water or elution buffer, and then analyzed by nanodrop to determine concentration. RNA concentration was generally standardized to 100 ng/µL or 250 ng/µL. Purified total RNA (1–2 µg) was used immediately for first strand cDNA synthesis or otherwise stored at − 80°C. Purified RNA was reverse transcribed into cDNA using Superscript IV First Strand Synthesis Kit (Thermo Fisher) according to the manufacturer's protocol. To ensure that cDNA was generated from only messenger RNA, we opted for the oligo d(T) primer during synthesis. Samples were stored at − 20°C until qPCR analysis.

2.5. Quantitative PCR primers

The following primer sets were used for amplification of *MYO7A, Myo7a*, or housekeeping genes:

hMYO7A qPCR IF1&2 Forward:	5′-CCCAAGAACGACGTCATC-3′.
hMYO7A qPCR IF2 Reverse:	5′-GTTTTCGCTCCCCTGCT-3′.
hMYO7A qPCR IF1 Reverse:	5′-GCAGCACAGCCAAGATCA-3′.
hHPRT Reverse:	5′-CCCTGTTGACTGGTCATTACA-3′.
hHPRT Forward:	5′-GGAGGCGATCACATTGTA-3′.
mMyo7a IF1&2 Set 1 Reverse:	5′-CCAGCAGGGTTAGGATTGT-3′.
mMyo7a IF1 Set 1 Forward:	5′-GGGCTGTGCTACTTGTCAA-3′.
mMyo7a IF2 Set 1 Forward:	5′-GTGTCCAGCAGTAGGGGAACA-3′.
mMyo7a IF1 Set 2 Forward:	5′-CCCAAGAGCGACGTCATC-3′.
mMyo7a IF1 Set 2 Reverse:	5′-GTAGCACAGCCCAAGTCAG-3′.
mHprt Forward:	5′-GGTGGAGATGATCTCTCAACTT-3′.
mHprt Reverse:	5′-CTGGCCTGTATCCAACACTT-3′.
pMyo7a IF1&2 Forward:	5′-AGCCTCCCCAAGAATGATGT-3′.
pMyo7a IF1 Reverse:	5′-CAGGACCAACACGAAGAACA-3′.
pMyo7a IF2 Reverse:	5′-GGTTCGCTCCCCTGCT-3′.
pHprt Forward:	5′-GGACTTGAATCATGTTTGTG-3′.
pHprt Reverse:	5′-CAGATGTTTCCAAACTCAAC-3′.

2.6. Quantitative PCR standardization

MYO7A and *Myo7a* primers were designed to span exon-exon junctions specific to each isoform to ensure that amplification was isoform specific, as well as to avoid amplification of genomic DNA. Standard curves were performed with each *MYO7A* or *Myo7a* primer set to ensure resulting data were not biased by differences in primer efficiency. Two types of mouse samples were used as template: mouse RPE cDNA, or, alternatively, full length *Myo7a* cloned into a pTOPO backbone plasmid. Full length *Myo7a* was PCR amplified from mouse RPE cDNA and the PCR products were cloned into a plasmid backbone using the Zero Blunt™ TOPO™ PCR Cloning Kit (Invitrogen). Clones were screened by Sanger sequencing (Laragen, Culver City, CA) to obtain isoform specific template vectors. The resulting templates (pTOPO-mus*Myo7a*-IF1, pTOPO-mus*Myo7a*-IF2) were prepared using PureLink™ Quick Plasmid Miniprep Kit (Invitrogen). Human samples from previously prepared plasmid DNA, containing either *MYO7A* IF1 or IF2, were also tested (pUH-CBA-mCherry-MYO7A-IF1, pUH-CBA-mCherry- MYO7A-IF2). The qPCR reactions were prepared in triplicate with each serial dilution, as follows: 1 µL DNA template, 1 µL 10 µM Forward and Reverse primer, 10 µL SYBR Green Master Mix, and 8 µL Ultrapure RNase-free water for a total of 20 µL per reaction. Samples were loaded into individual wells of a 96-well qPCR plate and analyzed using the Quant Studio 3 Pro Real-Time PCR System (Applied Biosystems). Ct values were averaged for each sampling group and plotted against the log of the DNA copy number. (Supplemental Fig. 2) Amplification efficiencies were calculated (Eff = 10(-1/slope) – 1) and recorded beneath each plot.

2.7. Quantitative PCR primer isoform specificity

Quantitative PCR analysis using templates made of pure isoform-specific cDNA plasmids at different concentrations, as well as mixtures of both IF1 and IF2 cDNA plasmids at various ratios were conducted for each primer set. The qPCR conditions used in the actual experimental conditions, as described above, were used. The average Ct value for each condition is the mean of three technical replicates.

2.8. Quantitative PCR analysis

Quantitative PCR amplification was performed using SYBR Green Master Mix (Applied Biosystem or BioRad). Fluorescent detection of PCR amplification was analyzed using Quant Studio 3 Pro Real-Time PCR System (Applied Biosystems) or LightCycler 480 Real-Time PCR Thermal Cycler (Roche), or Q qPCR instrument (Quantabio) with the following program: 50 ◦C for 2 min, 95 ◦C for 10 min, 40 cycles of 95 ◦C for 15 sec followed by 60 ◦C for 1 min. Melt curve analysis was performed to determine specificity of each PCR reaction, as follows: 95 ◦C for 15 sec, 60 ◦C for 1 min, and then 10 sec incremental incline of 1 ◦C, up to 95 ◦C. The housekeeping gene, *HPRT*, was used as an internal control. The relative expression of *MYO7A* IF1 and IF2 was determined by calculating ΔΔCt, normalized to *HPRT* expression. The Ct value was determined for each PCR reaction by automated threshold analysis by the PCR instrument, Quant Studio 3 Pro Real-Time PCR System (Applied Biosystems), LightCycler 480 Real-Time PCR Thermal Cycler (Roche), or Q qPCR instrument (Quantabio). Samples containing impurities, as determined by melting curve analysis, were discarded from analysis. The value of each technical replicate within a sample group was calculated and normalized to the housekeeping gene as such: ΔCt

(*MYO7A*) = Ct(*MYO7A*)- Ct(*HPRT*). The ΔΔCt was calculated from the difference in each normalized *MYO7A* ΔCt, as ΔΔCt = ΔCt(*MYO7A* IF1) - ΔCt(*MYO7A* IF2). Finally, the relative expression of each isoform was represented by 2- ΔΔCt .

2.9. Quantitative PCR sample sizes

As shown in Table 1, eleven mouse neural retina samples, each consisting of two pooled retinas, and four mouse RPE samples, each consisting of tissues pooled from four mice, were collected for analysis. An NR and RPE sample were each collected from two pig eyes. Seven wells of ARPE-19 were each independently polarized and harvested for analysis. Four cultures of differentiated RPE from xcHUF1 hiPSCs, and two cultures from hESCs were sampled. Data collected from stem cell-derived RPE samples were combined into a single group (iPS/ES-RPE) for analysis. Five groups of retinal organoids were used for analysis, each group containing a pool of six organoids. Four biological replicates of ro- RPE were used for analysis. Two de-identified post-mortem human subject eyes were collected, one each from two adult subjects. Both NR and RPE were sampled from the 42-year-old subject, while just the RPE was sampled from the 90-year-old subject. Between three and six technical replicates were used for each data point, depending on the RNA yield of each sample.

2.10. 3D modeling

3D models were generated by the Pymol software (https://pymol. org/2/). MYO7A FERM1 and FERM2 domains amino acid sequences were analyzed using the Phyre2 webserver (http://www.sbg.bio.ic.ac. uk/phyre2), or otherwise obtained from the Protein Data Bank (htt

ps://www.rcsb.org/). The resulting model (.pcb format) was imported into Pymol for 3D visualization analysis.

Table 1: Quantitative PCR samples.

Table 1
Quantitative PCR samples.

	Mouse NR	Mouse RPE	Pig NR	Pig RPE	ARPE-19	iPS/ES-RPE	Retinal Organoid	ro-RPE	Adult Human NR	Adult Human RPE
gender	M + F	M + F	F	F	M	M + F	F	F	M + F	M
no. of subjects*	11	4	1	1	–	–	–	–	2	1
no. of separate samples (n value)	11	4	2	2	7	6	5	4	2	1
no. of qPCR reactions per sample	3–4	6–9	6	6	4–6	3–8	3–6	3–6	3	3

* Two eyes were collected from each mouse or pig. Each pair of mouse eyes was pooled.

Results

In a screen of a human retinal cDNA library, multiple independent clones were found to represent one of two isoforms of *MYO7A*, which differed by the presence or absence of a 114-bp region (Weil et al., 1996). We detected these two isoforms in full length *Myo7a* or *MYO7A* PCR amplicons from mouse, pig and human RPE samples, using Sanger sequencing (Suppl. Fig. 1A). After cloning these cDNA libraries to generate pure isoform-specific constructs, we sequenced individual clones to determine the frequency of clones containing each isoform. In mouse RPE, we detected 1 clone containing the larger isoform and 5 independent clones containing the 114-bp deletion. In human RPE, we detected 2 independent clones of the larger isoform and 12 of the smaller isoform (Suppl. Fig. 1B). We refer to the larger isoform as IF1, and the smaller as IF2.

Fig. 1A depicts the domains of MYO7A and illustrates that the two isoforms differ from each other by a 38-amino acid sequence that is present in IF1 but not IF2. The presence or absence of this sequence is due to alternative splicing of exon 35, and it affects the structure of the FERM1 domain in the MYO7A tail (Fig. 1).

FERM domains are common protein binding regions (Chishti et al., 1998), so that any changes in these regions are likely to affect specific protein function. Some binding partners to the FERM1 domain of MYO7A have been reported, including another Usher 1 protein, SANS (Adato et al., 2005). To investigate the structural implications of modifying this domain, 3D models of each isoform were generated. These models revealed differences in the amino acid sequences at the tip of one loop of the C-lobe of the FERM1 domain. The differences appear to affect the opening to the cleft created between different lobes, and are thus likely to result in different protein interactions between IF1 and IF2 (Fig. 1D).

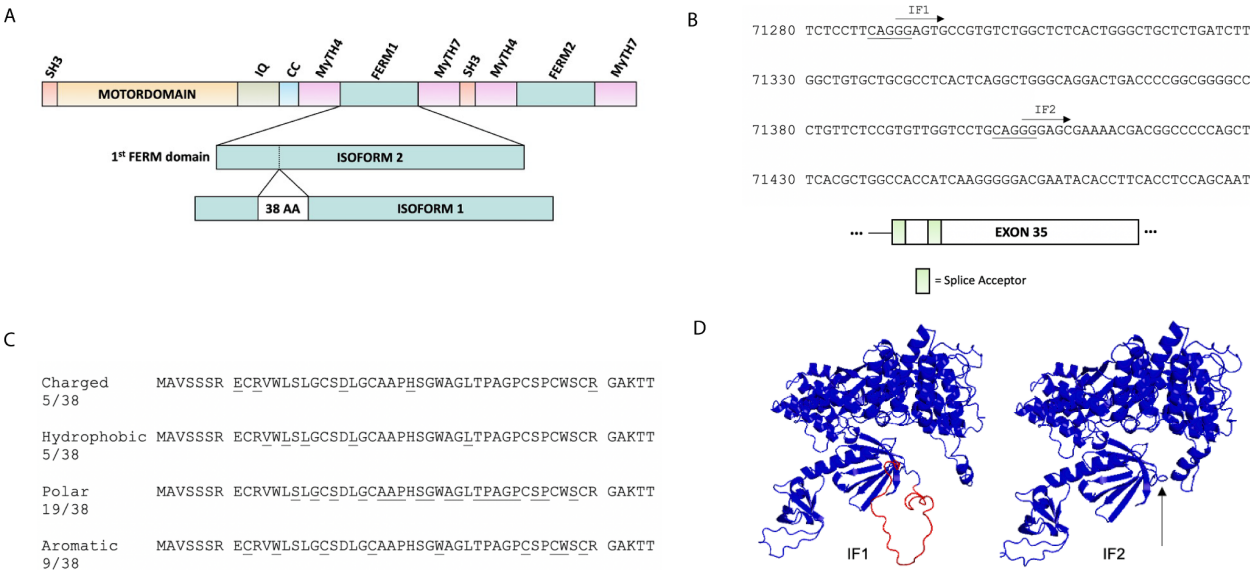

Fig. 1. The two retinal isoforms of MYO7A. (A) Schematic of MYO7A, illustrating the major domains of the polypeptide and the difference between the two retinal isoforms, which consists of the presence or absence of a 38-amino acid sequence within the FERM1 domain. (B) Depiction of the two putative IF1/IF2 splice acceptors that are associated with exon 35. The end of each putative splice acceptor sequence (YnNCAGGG) is underlined, and the first 6 nucleotides of each isoform coding region is marked with a directional arrow. (C) Amino acids of the 38-amino acid sequence that is unique to IF1, identified by class. (D) 3D modeling of the FERM1 domain of human MYO7A IF1 and IF2. The additional 38 amino acids at the C lobe of the FERM1 domain of IF1 are marked in red, and the location where they are missing in IF2 is marked with an arrow.

In the retina, MYO7A has been detected in the RPE and the photoreceptor cells of rodents and humans by immunocytochemistry (Hasson et al., 1995, Liu et al., 1997). Mutant phenotypes in mice, lacking functional MYO7A, confirm this localization by showing functions for MYO7A in both these cell types (e.g. Liu et al., 1998, Liu et al., 1999). Single cell RNA sequencing of human retinal organoids has also detected the expression of MYO7A in Müller cells and on-bipolar cells (Leong et al., 2022), although no MYO7A protein has been demonstrated in these cells.

To determine the relative abundance of each isoform in RPE and neural retina (NR, including the photoreceptor cells), we compared the relative expression of IF1 and IF2 in a variety of RPE and NR samples from mouse, pig, and human. The mouse and pig samples consisted of freshly dissected post-mortem retinas. The human RPE samples included cultures of polarized monolayers that were differentiated from 1) the ARPE-19 cell line, 2) human embryonic stem cells (hESCs), and 3) human induced pluripotent stem cells (hiPSCs). The human NR samples included retinal organoids that were generated from hiPSCs. Human RPE samples were also isolated and further differentiated from the retinal organoids (ro-RPE). In addition, we tested NR and RPE from human post-mortem eyes.

To ensure the comparison of IF1 and IF2 expression level would not be skewed by a difference in primer efficiency, we generated standard curves for human and mouse primer sets using species- and isoform-specific cDNA constructs. Due to the short sequence difference between the two isoforms (114 bp), primer design options were limited. However, the primers we selected had a comparable efficiency between IF1 and IF2 for each species (0.77 and 0.79 for mouse, and 0.83 and 0.85 for human, Suppl. Fig. 2). To further test the specificity of each primer set, we conducted qPCR analysis using a mixture of both isoform-specific cDNA plasmids; we found relatively negligible amplification of the non-targeted isoform template at the measured expression ratios (Supplementary Tables 1 and 2).

The ratio of IF1 to IF2 was relatively consistent for the different human and pig samples tested (Fig. 2). IF2 was the predominant isoform expressed in human RPE and NR samples, accounting for 82–90% of the relative *MYO7A* expression. A similar isoform ratio was found in pig tissues, with IF2 accounting for the majority of expression in both the RPE (89%) and NR

(90%). On average, IF1 accounted for about 1 in 7 of *MYO7A* transcripts across pig and human samples, a ratio that is consistent with the frequency of isoform-specific clones from the human samples (Suppl. Fig. 1B). In mouse RPE, IF1 was still the lower expressed isoform, but accounted for a larger relative proportion of *Myo7a* transcript (23%). In contrast, mouse NR showed higher expression of IF1 than IF2 expression (52 vs 48%).

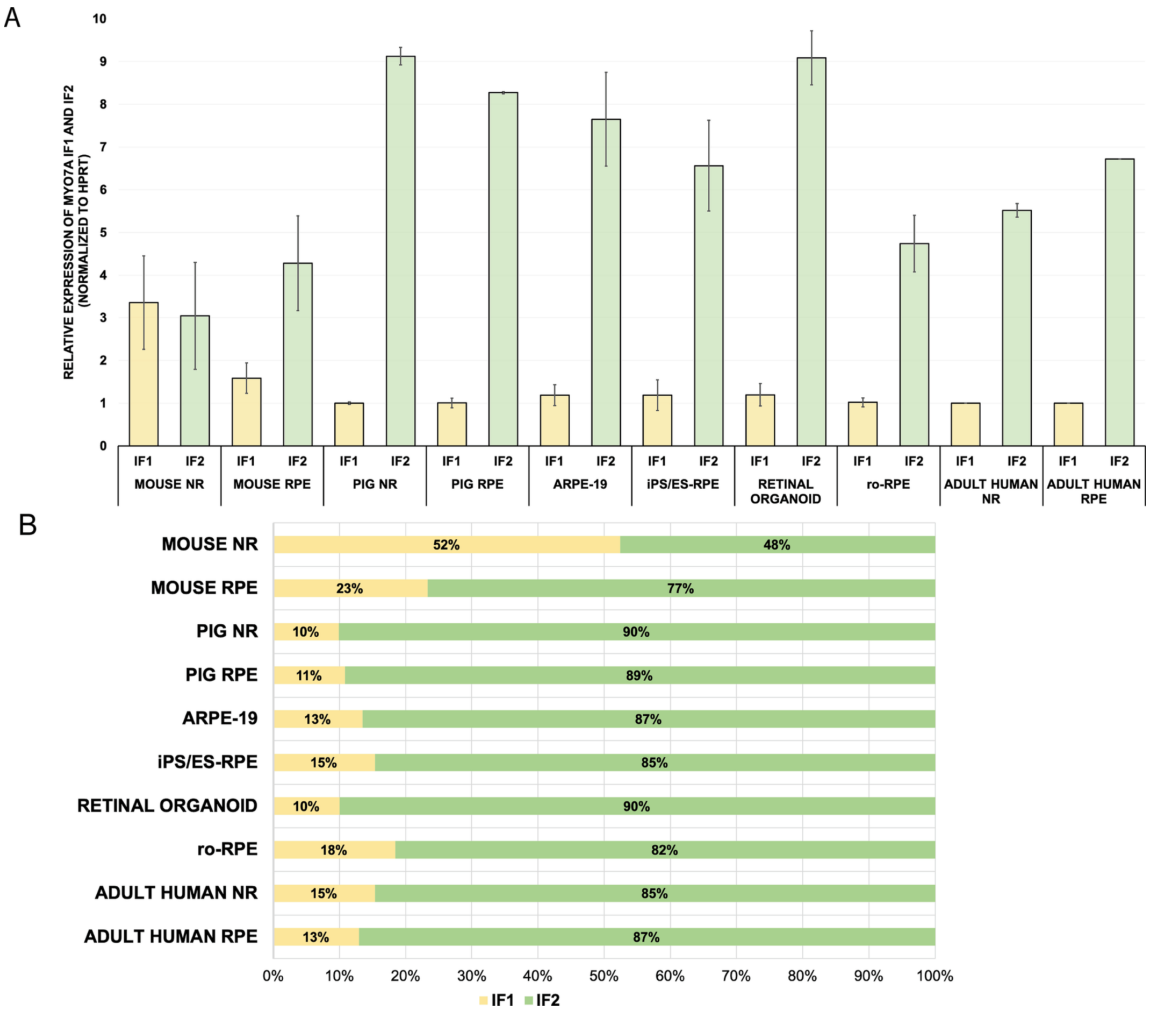

Discussion

Like most of the other Usher syndrome genes (Williams et al., 2017), *MYO7A* is alternatively spliced, with two major isoforms expressed in the retina (Weil et al., 1996). Using

quantitative PCR, we measured significant expression of both these two isoforms in the NR and RPE of human, pig and mouse. In human and pig NR and the RPE of all three species, the expression of IF2 was greater than that of the longer isoform, IF1. In mouse NR, IF1 expression was more comparable to that of IF2. Irrespective of the relative expression levels of the two isoforms, an important point from our study is that significant levels of both isoforms were detected in both the NR and the RPE of three different mammals. This finding suggests that both IF1 and IF2 of MYO7A likely function in the developed NR and RPE, so that gene augmentation therapy attempts with a single isoform might be of limited success.

4.1. Retinal MYO7A isoforms in relation to gene augmentation therapy

The first clinical trial to prevent USH1B blindness used gene augmentation therapy with *MYO7A* IF2. Based on our relative expression data, this more highly expressed isoform would seem to have been a more prudent choice if only one isoform were to be used. The human IF2 construct was provided by our lab to Oxford Biomedica for incorporation into an EIAV lentiviral vector for subretinal delivery. This trial was abandoned before efficacy could be assessed properly. Nevertheless, earlier, HIV lentiviral delivery of the same IF2 construct had been shown to correct some of the known mutant phenotypes due to lack of MYO7A function in mouse retinas. Correction was determined by the localization and motility of RPE melanosomes, the degradation of photoreceptor outer segment phagosomes, and the concentration of opsin in the connecting cilia of the photoreceptor cells (Hashimoto et al., 2007). *Myo7a*-mutant mice manifest mislocalized melanosomes in the apical RPE, due to aberrant motility (Liu et al., 1998, Futter et al., 2004, Gibbs et al., 2004), slowed phagosome degradation, due to impaired

movement of the nascent phagosomes from the apical RPE (Gibbs et al., 2003, Jiang et al., 2015), and an abnormal accumulation of opsin in the connecting cilia of photoreceptor cells (Liu et al., 1999). However, lack of MYO7A also results in several additional mutant phenotypes, which suggest other functions (Williams & Lopes, 2011). Electrophysiological studies of *Myo7a*-mutant mice showed a slightly reduced a- and b-wave response (Libby & Steel, 2001). With mutant mice on a different genetic background, a more significant electroretinogram abnormality was observed, including a delay in the recovery of rod responsiveness after desensitization (Colella et al., 2013). In the RPE, MYO7A is also required for the light-dependent translocation of the retinoid isomerase, RPE65, with mice that lack MYO7A having lower overall levels of RPE65, as well as mislocalization of the isomerase (Lopes et al., 2011). Correction of these phenotypes was not tested in the initial gene augmentation studies in mice (Hashimoto et al., 2007); nor were they tested in a later study using the same IF2 cDNA, but delivered by AAV (Lopes et al., 2013). Interestingly, gene augmentation studies with *Myo7a*-mutant mice, using a cDNA of human *MYO7A* IF1, have demonstrated correction of some of the same phenotypes that were corrected by human *MYO7A* IF2. Melanosome localization in the apical RPE was corrected with human *MYO7A* cDNA that was reported to be IF1, packaged in either single or dual AAV vectors. (Colella et al., 2013, Trapani et al., 2014, Ferla et al., 2023) This treatment also improved the electrophysiological recovery from light desensitization (Colella et al., 2013). The correction of melanosome localization with either IF1 or IF2 is consistent with the reported interaction between MYO7A and melanosomes in the RPE. Melanosome motility by MYO7A is mediated by association of RAB27A on melanosomes with the exophilin, MYRIP, which in turn binds to a region of the tail of MYO7A (El-Amraoui et al., 2002, Fukuda & Kuroda,

2002, Klomp et al., 2007, Lopes et al., 2007). This tail region of MYO7A is identical between MYO7A IF1 and IF2. It includes the FERM2 domain, but it does not include the FERM1 domain, which is where the two isoforms differ. (Fig. 1) The requirement of the MYO7A FERM2 tail region for melanosome motility and localization has been demonstrated in vivo, using *Myo7a*-mutant mice, known as *polka*. *Polka* mice carry a splice site mutation (c.5742 + 5G > A) that results in a MYO7A protein, truncated at the FERM2 domain. In the RPE of *polka* mice, the mutant MYO7A protein is present at WT levels, but it does not associate with melanosomes, resulting in their mislocalization. (Schwander et al., 2009) Functions that involve protein or organelle association with the FERM1 domain of MYO7A are more likely to be specific for IF1 or IF2. In this respect, the scaffolding protein, SANS, has been shown to bind the FERM1 domain of MYO7A. (Adato et al., 2005) Mutations in *SANS* underlie USH1G (Weil et al., 2003), and SANS-MYO7A binding is thought to be part of a network of USH1 proteins (Adato et al., 2005, Reiners et al., 2005), and perhaps involved in ciliary transport. (Sorusch et al., 2019) In summary, MYO7A IF1 and IF2 are likely to have overlapping functions (e.g. melanosome motility and localization), in addition to distinct functions that involve the FERM1 domain. Although gene augmentation experiments with either IF1 and IF2 have corrected some mutant phenotypes in mice (Hashimoto et al., 2007, Lopes et al., 2013, Colella et al., 2014), correction of other mutant phenotypes has not been demonstrated. These other mutant phenotypes may result from loss of one specific isoform. To our knowledge, there are no known USH1B mutations that would affect just one *MYO7A* isoform. Nevertheless, two mutations in the IF1-specific region, a nonsense mutation, W1558X, and a frameshift mutation (2-bp deletion), C1554fs, have been reported by ClinVar (but with no ophthamological information); ClinVar is hosted by the

National Center for Biotechnology Information (NCBI). With the possibility of requiring IF1 or IF2, specifically, to correct a mutant phenotype (due to function related to the FERM1 domain of MYO7A), it seems prudent, to design a gene augmentation therapy that includes both isoforms. One approach would be to test a single construct with IF1 cDNA that includes intron 34 (0.9 kb), to potentially generate both IF1 and IF2 through alternative splicing (Fig. 3). An alternative approach would be to employ gene editing, rather than gene augmentation. In general, gene editing assumes an advantage over gene augmentation when a gene expresses more than one isoform. A paper in this *Vision Research* special edition (Yan et al., 2023) argues for additional advantages. However, USH1B mutations are present in all parts of the *MYO7A* gene, with no particular mutation showing a high frequency (Jacobson et al., 2011), so that a significant advantage of a well-designed gene augmentation therapy for USH1B is that it should provide one treatment for all cases, whereas gene editing would not.

4.2. Both the RPE and photoreceptors as necessary targets for USH1B gene therapy

Previously, we reported that the photoreceptors might be the initial site of the USH1B disease, based on the first detection of cell pathology by in vivo imaging and the similarity of retinal pathology of USH1B with that of other Usher syndromes (Jacobson et al., 2008). However, more advanced imaging of RPE cells may have detected RPE pathology earlier. In any case, there are two fundamental reasons that suggest there is a need to address both the RPE and photoreceptors in USH1B gene therapy. First, MYO7A protein, as well as mutant phenotypes in its absence, have been detected in both mammalian RPE and photoreceptors (Hasson et al., 1995, Liu et al., 1997, Liu et al., 1998, Liu et al., 1999). Second, the site of manifestation of pathology is not necessarily the site of the defective molecular mechanism that leads to the

evident pathology. There are several well-known examples among inherited RDs that involve cell nonautonomous impairment, particularly where a molecular defect in the RPE results in primary pathology in the photoreceptor cells; e.g. mutations in *MERTK* and *RPE65* (Mullen & LaVail, 1976, Gu et al., 1997). Moreover, the variety of mutant phenotypes due to a lack of MYO7A function in the retina suggests that these defects may collectively contribute to USH1B pathology. While these mutant phenotypes were largely discovered in mice, some have been corroborated in human RPE cells. For example, impaired degradation of phagosomes was shown in *MYO7A*-deficient human RPE cells. (Gibbs et al., 2010) This particular cellular RPE defect is a good candidate for contributing to a general insult that leads to USH1B pathology, since it has been linked to RD through mutations in other genes. (Rakoczy et al., 2002, Krock et al., 2007, Gordiyenko et al., 2010, Jiang et al., 2015, Esteve- Rudd et al., 2018) Therefore, it seems clear that we should treat both the photoreceptors and the RPE in USH1B in any planned gene therapy and, as noted above, the expression of MYO7A IF1 and IF2 in both the RPE and the NR indicates that treatment should address both isoforms. A question remains whether additional retina cell types should also be targeted. The detection of *MYO7A* gene expression in other retinal cells, by single cell RNA sequencing of human retinal organoids (Leong et al., 2022), suggests that these other cells, especially the Müller cells which provide a supportive role to the photoreceptors (Reichenbach et al., 1993), might also be a necessary target for complete retinal gene therapy.

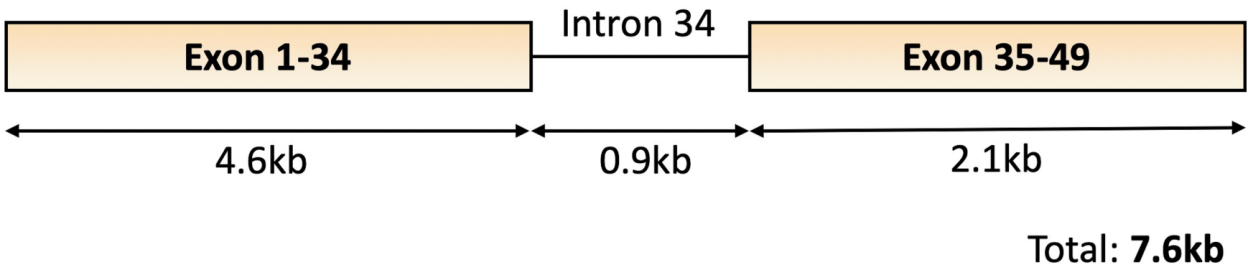

Fig. 3. Suggested construct design that would potentially generate both IF1 and IF2 MYO7A isoforms in gene augmentation therapy.

4.3. Comparative localization of MYO7A in the photoreceptors

An early low magnification immunolabeling study of mouse photoreceptors failed to detect MYO7A (El-Amraoui et al., 1996), and a recent paper also concluded that MYO7A was absent from mouse photoreceptors (Calabro et al., 2019). However, immunoEM studies have not only been able to detect MYO7A in the connecting cilium, but also demonstrate the abnormal accumulation of opsin in this region in *Myo7a*-mutant mice, thus associating a mutant phenotype due to loss of MYO7A function with mouse photoreceptors. These EM results have now been verified independently by at least 4 different laboratories (Liu et al., 1997, Liu et al., 1999, Hasson, 2000, Wolfrum & Schmitt, 2000, Colella et al., 2013). Moreover, using female *Myo7a*-null mice, expressing a *Myo7a* transgene from their X-chromosome, it was demonstrated that the mutant phenotype of abnormal opsin accumulation in the connecting cilium is due to lack of MYO7A in the photoreceptor cells themselves and not from lack of MYO7A in the RPE cells; the retinas of these mice contained mosaics of MYO7A-null and MYO7A-positive photoreceptor and RPE cells (Jacobson et al., 2008). ImmunoEM suggests that the localization of MYO7A to the photoreceptor connecting cilium is similar between human and rodents (Liu et al., 1997). However, MYO7A is also localized to the photoreceptor calycal

processes, together with other USH1 proteins (Sahly et al., 2012), and the organization of the calycal processes differs significantly between mouse and human. A calycal process is an f-actin-filled extension from the inner segment that associates with the proximal region of the outer segment. Mouse and rat rod photoreceptors have been shown to possess at least a single calycal process (Kessel & Kardon, 1979, Arikawa et al., 1992, Volland et al., 2015). However, they do not possess the array of many calycal processes that surrounds the basal region of the outer segments of primates, pigs, frogs, and many other vertebrates (Brown et al., 1963, Hogan et al., 1971, Steinberg et al., 1980). Calycal processes require actin filaments for their organization. When f-actin is depolymerized, they collapse, and this collapse was suggested to contribute to defective disk membrane morphogenesis that is manifest by overgrown nascent disks (Williams et al., 1988). Loss of PCDH15 or CDH23, the USH1F and USH1D proteins, also results in loss of f-actin in the calycal processes and the same perturbed disk morphogenesis phenotype (Schietroma et al., 2017). Hence, the calycal process localization of USH1 proteins may be important in USH1 retinal pathology (Sahly et al., 2012, Schietroma et al., 2017), although, to date, no mutant phenotype has been linked to the calycal processes due to lack of MYO7A. We found the expression of *Myo7a* IF1 to be more similar to that of IF2 in mouse NR, whereas in pig or human NR, IF2 is clearly the more abundant isoform (Fig. 2). These results were confirmed using a second set of mouse IF1 primers. It is tempting to suggest that this difference in isoform expression might be related to a difference between mouse and human in the photoreceptor subcellular structures that contain MYO7A, combined with different subcellular distributions for IF1 and IF2. However, photoreceptors in retinal organoids do not appear to have well-developed calycal processes, even in the few cases where disk membranes

(rather than membrane tubules) have clearly formed. (Zhong et al., 2014, West et al., 2022) Yet, the IF1 to IF2 ratio was similar between human retinal organoids and the other human retinal tissues (Fig. 2), suggesting no relationship between isoform expression and photoreceptor subcellular structures.

Chapter 2: Tools for Studying Myosin VIIa

Understanding the optimal approach for any therapy requires a deep understanding of the disease being treated. This is especially true for rare genetic diseases, where treatable patients are finite. A deep understanding of disease requires an understanding of how a system operates in its normal, healthy state. A clear understanding of disease-causing genes and the functions they play in tissues that require their expression to develop and operate normally enables researchers to hone in on the root causes of disease.

The work discussed in this chapter focuses on the development of new tools for studying the disease-causing gene found in patients with USH1B. We engineered and preliminarily validated a set of tools that will allow us to explore the functional roles of each MYO7A isoform and better understand their potential differences. This work also aims to highlight the importance of different gene isoforms and the roles they play in the retina.

Myosin VIIa in the Retina

Myosins are mechanoenzymes that interact with actin and ATP to generate motility. They are involved in a wide range of cellular functions, including cell division, trafficking, and organelle movement. Myosin VIIa is an unconventional myosin with various functions, including intracellular trafficking and structural support for critical sensory cells in the inner ear and retina. *MYO7A* was the first USH gene to be cloned. (Gibson et al, 1995; Weil et al., 1995) In the human genome, it is located on the long arm of chromosome 11 in sub-band 5 of region 13 (11q13.5). (Kelley et al., 1997) It spans 120 kilobases and includes 49 exons, (Kelley et al., 1997)

with the largest isoform having a 6642 base pair coding region. *MYO7A* expression has been detected in a range of tissues, with enhanced expression in certain tissues. *MYO7A* encodes Myosin VIIa protein. The primary functional components of the protein are an N-terminal motor head domain and a cargo-binding tail. (Inoue 2003) The motor domain consists of an actin binding region, a large ATPase, and a calmodulin-binding IQ domain. (Udovichenko et al., 2002) The tail consists of two MyTH4-FERM domains (MF1 and MF2) in tandem, linked by a Src homology 3 (SH3) motif. These domains mediate interactions between Myosin VIIa and other proteins, such as Sans (Wu et al., 2011), Cdh23 (Bahloul et al 2010), and MyRIP. (El-Amraoui, 2002) It is likely that additional associations and binding partners to the Myosin VIIa tail are still unknown. As discussed in Chapter 1, two *MYO7A* isoforms are expressed in the retina, which differ by a 38 amino acid sequence absent in IF2. Whether the presence or absence of this sequence leads to functional differences between each isoform remains unknown. If so, this could have critical implications for *MYO7A* gene augmentation therapy.

To explore potential function differences of the major *MYO7A* isoforms (IF1 and IF2), we generated a set of versatile molecular tools for our studies, hereafter referred to as "MYO7A tools." A red fluorescent tag was added to the N-terminus of each IF1 and IF2 by cloning an mCherry gene to the 5' end of the *MYO7A* gene. Since the N-terminus Myo7a consists of domains critical for motor activity, fusion of the fluorescent tag required flexible glycine- and serine-rich linker peptides in order to avoid interfering with protein function. These constructs are driven by a strong, constitutive promoter (CAG) in a 3rd generation lentiviral backbone.

An additional set of constructs was generated to study both major *MYO7A* isoform tail domains. (Fig. 4B) Removal of the N-terminal actin-binding and motor domains from Myosin

VIIa results in a “free ranging” tail capable of targeting binding partners less accessible by the full-length protein. Replacement of the head domain with a fluorescent tag further improves the utility of these tools for a broader spectrum of functions, including spatial and temporal tags for Myosin VIIa cargo. Use of these tools could help better elucidate the *MYO7A* interactome across a range of tissues.

Assembly of Myosin VIIa Research Tools

CBA-mCherry-*MYO7A* Vector Construct Cloning

A lentiviral fluorescently-tagged *MYO7A* isoform 2 construct was assembled by a 3-step cloning process. Full length *MYO7A* isoform 2 was PCR amplified from human H9-RPE cDNA (Platinum SuperFi PCR Kit, Invitrogen), purified (PureLink PCR Purification Kit, Invitrogen), and cloned into pTOPO backbone (Zero Blunt TOPO PCR Cloning Kit, Introgen). Next, A CAG promoter (chick beta actin promoter with cytomegalovirus enhancer), an mCherry gene, and *MYO7A* IF2 gene were PCR amplified, and cloned into a EcoRI and BamHI digested pUC18 backbone. Finally, the entire CBA-mCherry-*MYO7A* IF2 construct was PCR amplified and cloned into an SpeI and KpnI digested pUltraHot lentiviral backbone (plasmid #24130, AddGene). In order to switch the genetic isoform 1 of *MYO7A* in this vector, an additional cloning step was required. A synthetic gene block (IF1 gene block) was inserted into a ScaI and BspEI digested pUH-CBA-mCherry-MYO7A IF2 plasmid.

Cloning *MYO7A* Tail Vectors

A CMV-eGFP-*MYO7A* isoform 2 tail construct was acquired from a collaborating lab. This construct was cloned into an SpeI and KpnI digested pUltraHot lentiviral backbone. A lentiviral mCherry-CMV-*MYO7A* IF1 tail construct was generated using a similar approach to the full length *MYO7A* constructs. A CMV promoter, an mCherry gene, and *MYO7A* IF1 tail gene were PCR amplified, and cloned into a EcoRI and BamHI digested pUC18 backbone. The entire CMV-mCherry-*MYO7A* IF2 construct was PCR amplified and cloned into an SpeI and-KpnI digested pUltraHot lentiviral backbone.

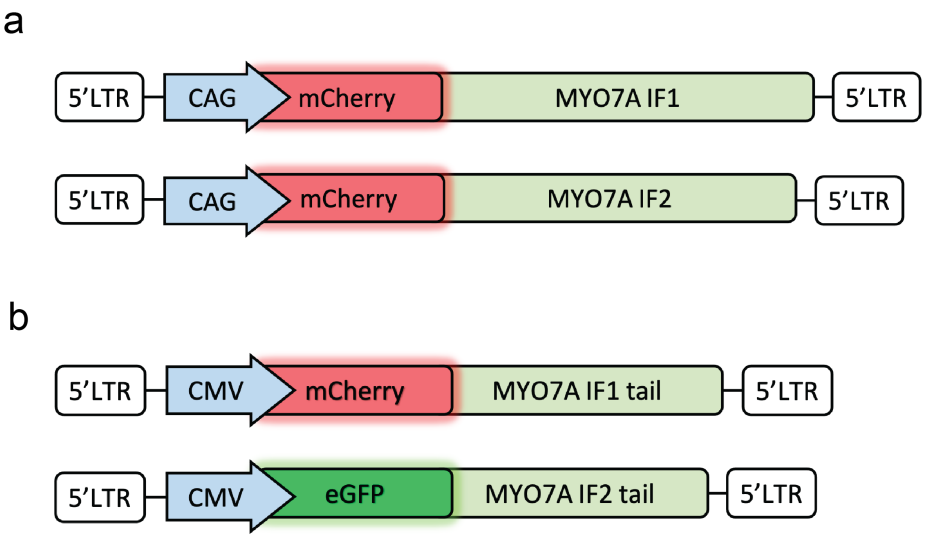

Figure 4: Illustration of MYO7A tools. A) Full length MYO7A constructs consist of *MYO7A* IF1 or IF2 fused to an mCherry gene. These are driven by a CAG promoter in a lentiviral backbone. B) Tail constructs are composed of the 3' tail domains of *MYO7A* IF1 and IF2 fused to either eGFP or mCherry. These are driven by a CMV promoter in a lentiviral backbone. Tail domains spanned from MF1 domain to the end of the gene - MyTH4-end (c.2895-7397) for IF1 tail and FERM1-end (c.3799-7284) for IF2 tail.

Methodology and Implications for Research Use

Application of these tools for research done in a number of ways. Delivery by lentivirus is a simple and effective way to generate cell line models. Stable expression of these constructs can help identify spatial and temporal localization of Myosin VIIa when used in conjunction with fluorescent live cell imaging. Co-immunoprecipitation using anti-GFP or anti-mCherry antibodies can be used to identify binding partners of Myosin VIIa across a range of tissues. The below discussion is dedicated to possible applications of the MYO7A tools generated during my research.

Applications for Studying RPE Function

As previously discussed, *MYO7A* plays a role in multiple primary functions by the RPE. Absence of *Myo7a* leads to abnormal phagocytosis phenotype, (Williams and Lopes, 2011) though its involvement in the specific processes involved in RPE phagocytosis are still unclear. Application of the MYO7A tools to well-established in vitro models of POS phagocytosis by the RPE could enable further investigation into this gap in knowledge.

Additional functions of *MYO7A* in the RPE are also possible. One common symptom found in USH1B patients is macular edema. The connection between *MYO7A* and the build-up of fluid deposits in the macula is unclear, though it is possible that absence of functional *MYO7A* could impair other primary functions of the RPE, such as epithelial transport and integrity of the outer retina barrier. These tools could help explore the connection between *MYO7A* and critical functions of the RPE.

Applications for Hearing Research

Myo7a is known to play a role in cochlear stereocilia organization, from experiments performed in the shaker-1 mouse. (Lau et al., 2023). It is not clear whether USH1B-associated hearing loss is due to abnormal development issues of the inner ear or the requirement of *MYO7A* expression for sensory cell function. These tools could be applied by stem cell researchers to address this gap in knowledge. Cochlear tissues can be differentiated from human induced pluripotent stem cells (iPSCs). (Moore et al., 2023) USH1B patient-derived iPSCs stably expressing MYO7a tools could be differentiated into cochlear organoids, and assessed for morphological and phenotypic differences compared to the diseased line. Use of these tools to study the spatial localization and activity of Myosin VIIa in cochlear cell models, and the protein's involvement in morphological and structural differences seen in diseased cells could provide valuable insight into the biology of inner ear and the disease pathology of USH1B-associated hearing loss.

Limitations

One limitation of the tail constructs is the CMV promoter, which may be suppressed in some cell types. Fortunately for using these tools to study *MYO7A* in the RPE, the CMV promoter is typically not an issue. These tools could be optimized by swapping the promoter with the endogenous gene promoter of *MYO7A*. This could alleviate the potentially toxic effects of overexpression, which has been reported. (Hashimoto et al., 2007)

Additional Material

Table 2: Cloning primers

PRIMER NAME	SEQUENCE
<u>pUC18-CAG-mCherry-MYO7A IF2 Assembly</u>	
CAG fwd	TAAAACGACGGCCAGTGCCAAGTTCCGCGTTACATAACTTACGGTAAATGGCCCGCC
CAG rev	GGTGGACTAGTCATGCAAGCTTTCTAGAGTCGACAGCGACTCCCGCCCGCCGCGCGCTTCG
mCherry fwd	TAAAACGACGGCCAGTGCCAAGTTCCGCGTTACATAACTTACGGTAAATGGCCCGCC
mCherry rev	GGTGGACTAGTCATGCAAGCTTTCTAGAGTCGACAGCGACTCCCGCCCGCCGCGCGCTTCG
MYO7A fwd	TCCGGAAGTGCTGGGAGCGCAAGCGGAAGCGGAGGCTCCGGTATGGTGATTCTTCAGCAGGGG
MYO7A rev	CAGCTATGACCATGATTACGTCACTTGCCGCTCCTGGAG
<u>pTOPO-MYO7A IF2 Assembly</u>	
MYO7A NT Fwd	GGACCATGGTGATTCTTCAGC
MYO7A CT Rev	TCACTTGCCGCTCCTGGAG
<u>pUH-CAG-mCherry-MYO7A IF2 Assembly</u>	
CAG mCh-MYO7A Fwd	AGAGATCCAGTTTGGTTAATAGTTCCGCGTTACATAACTTACGG
CAG mCh-MYO7A Rev	GTCATTGGTCTTAAAGGTACTCACTTGCCGCTCCTGGAG

IF1 gene block sequence:

TGAGCTGGCCTCCCAGCAGTACTTTGTAGACTATGGCTCTGAGATGATCCTGGAGCGCCTCCTGAACCTC
GTGCCCACCTACATCCCCGACCGCGAGATCACGCCCCTGAAGACGCTGGAGAAGTGGGCCCAGCTGGC
CATCGCCGCCCACAAGAAGGGGATTTATGCCCAGAGGAGAACTGATGCCCAGAAGGTCAAAGAGGATG
TGGTCAGTTATGCCCGCTTCAAGTGGCCCTTGCTCTTCTCCAGGTTTTATGAAGCCTACAAATTCTCAGGC
CCCAGTCTCCCCAAGAACGACGTCATCGTGGCCGTCAACTGGACGGGTGTGTACTTTGTGGATGAGCAG
GAGCAGGTACTTCTGGAGCTGTCCTTCCCAGAGATCATGGCCGTGTCCAGCAGCAGGGAGTGCCGTGTC
TGGCTCTCACTGGGCTGCTCTGATCTTGGCTGTGCTGCGCCTCACTCAGGCTGGGCAGGACTGACCCCG
GCGGGGCCCTGTTCTCCGTGTTGGTCCTGCAGGGGAGCGAAAACGACGGCCCCCAGCTTCACGCTGGCC
ACCATCAAGGGGGACGAATACACCTTCACCTCCAGCAATGCTGAGGACATTCGTGACCTGGTGGTCACC
TTCCTAGAGGGGCTCCGGAAGAGATCTAAGTATGTTGTGGC

Chapter 3: Base Editing Approach for Myo7a Gene Correction

Usher Syndrome

Usher Syndrome (USH) is a rare deaf-blindness disease, affecting at least 3 in every 100,000 persons. (Boughman, 1983) The disorder was first described in 1858 by German Ophthalmologist von Gräfe. (von Grafe, 1858) Clues of its origin as a genetic disease were described shortly after in 1861. (Liebreich et al, 1861) A half century later, the disease was named after Scottish ophthalmologist Charles Howard Usher who documented 69 cases of the disease. (Usher et al, 1914) USH was later categorized into three different subtypes based on severity and onset of clinical symptoms, including hearing impairment, vestibular dysfunction, and retinitis pigmentosa (RP). (Davenport & Omenn, 1977) Studies from the 1990's mapped the genetic loci associated with each USH subtype (USH1B (Kimberling, 1992; Smith, 1992), USH1C (Smith, 1992), USH1D (Wayne, 1996), USH1E (Chaib, 1997), USH1F (Wayne et al, 1997), USH1G (Weil et al., 2003; Kikkawa et al 2003), USH2A (Kimberling, 1990; Lewis, 1990), USH2C (Weston et al, 2004), USH2D (Ebermann et al., 2007), USH3A (Sankila, 1995)), leading to the subclassification of the disease according to the causative mutant gene.

USH Genetics and Clinical Symptoms

Usher syndrome type I (USH1), the most severe type, is linked to mutations in MYO7A, HARMONIN, CDH23, PCDH15, SANS, and CIB2 genes, resulting in profound hearing loss with vestibular dysfunction from birth, and early onset RP from the first decade. USH2, caused by mutations in USH2A, ADGRV1, and WRLN genes, involves moderate-to-severe congenital

hearing loss without vestibular dysfunction and postpubertal RP. USH3, caused by mutations of the CLRN1 gene, is characterized by progressive hearing loss with variable vestibular dysfunction and postpubertal RP. Atypical USH cases involve “ultra-rare” mutations in CEP78, (Namburi et al., 2016) HARS, (Puffenberger, 2012) PDZD7, (Ebermann et al 2010) ABHD12, (Eisenberger, 2012) CEP250, (Khateb 2014) ESPN, (Ahmed 2018), CIB2 (Riazuddin et al., 2012) and ARSG (Khateb 2018) genes. (Nolen et al, 2020)

USH Genes

USH genes are known to express in tissues within the inner ear and retina, where they play critical roles in establishing and maintaining sensory. The molecular mechanisms that underlie the formation and progression of disease are not well understood, however the work from several groups has elucidated some of the processes involved in USH disease pathology. Several USH genes are involved in creating structural components of scaffolding complexes that comprise critical sensory cells in the cochlea and retina. Mutations in any of these genes result in some degree of impairment to the development, structure, and/or function of the sensory organs comprising the affected cells. Some interactions between USH proteins have been discovered, and models for an USH-protein network interactome have been proposed. (Reiners, 2005) The varying degree of disease symptoms between different USH subtypes illustrates the relative importance of each gene for overall sensory system health. The pathomechanisms of USH disease (Reiners, 2006; Kremer, 2006; El-Amraoui, 2006; Adato, 2005; Maerker, 2008; Tian, 2009)

USH-associated hearing loss stems from defects of the inner ear. USH retinas undergo normal development; however, in some forms of USH, maintenance and upkeep of healthy tissue becomes an issue as early as adolescence, eventually leading to degeneration and vision loss. Within the retina, most USH genes express primarily in photoreceptors, with the exception of MYO7A, which expresses predominantly in the RPE. USH genes may affect additional systems of the body, however their relevance to disease remains unknown.

Usher Syndrome 1B

USH1B is the most common subtype of the most severe form of USH. The disease is caused by a wide range of inherited mutations along the gene. (Weston et al 1996; Adato et al 1997; Ouyang et al, 2005; Riazuddin et al, 2008; Jaijo et al, 2006; Jacobson et al., 2011) Disease symptoms present in the retina from early adolescence. These include decreased night vision and progressive constriction of visual field due to retinitis pigmentosa (RP), a clinical hallmark of retinal degeneration. By midlife, visual impairment is severe. Vision loss is severely detrimental to quality of life, especially when compounded with hearing and balance issues. The most optimistic clinical outlook for USH1B patients relies on early detection of disease-causing mutations in MYO7A and treatment intervention preceding the onset of RD.

Although there is currently no treatment available to prevent or reverse USH1B-associated RD, several active clinical trials and pre-clinical studies are currently underway to address the clinical need. Among these include gene and cell-based therapies, which aim to correct the genetic deficiency of MYO7A before the onset of disease or replace degenerated

parts of the retina with healthy tissue. (French et al., 2020) For the relevancy of this dissertation, the discussion will focus on gene-based therapies.

Disease Models

The appropriate disease model for USH1B depends on the focus of study. The most prominent disease model of USH1B is the shaker-1 mouse, (Gibson et al 1995) which carries mutant Myo7a in both alleles. These mice commonly exhibit some, but not all disease phenotypes seen in USH1B patients, such as balance issues due to vestibular dysfunction and profound deafness from birth. They do not, however, undergo retinal degeneration, though similar disease-associated phenotypes have been described in the tissues of the retina, particularly in the RPE. Such phenotypes include mis-localization of melanosomes (Liu et al, 1998; Gibbs et al., 2004) and impaired phagocytosis of ingested photoreceptor outer segments (Gibbs et al., 2003). Studies comparing these phenotypes in shaker-1 RPE and cultured human primary RPE have validated the significance of both for the study of USH1B. (Gibbs et al., 2010)

Tissue culture models of USH1B are an appealing alternative to the shaker-1 mouse since they circumvent the challenges of breeding diseased animals and should more accurately reflect the human disease phenotypes. USH1B patient-derived tissues are a promising disease model. Induced pluripotent stem cells (iPSCs) can be generated from USH1B patient fibroblasts. These can then be differentiated into tissue-specific cell lines, such as iPS-RPE, or miniature organelles, like retinal organoids. Only recently has the potential of USH1B patient-derived retinal organoids for studying disease pathology been described. (Leong et al., 2022)

In order to determine the best approach for Myo7a gene repair using base editing, we required a model for testing multiple variations of genetic repair constructs. This required abundant test samples and a quick-and-easy read-out of success. We engineered a specialized cell line that is suitable for our studies, hereafter referred to as “293T shaker reporter.”

Results

The 293T shaker reporter cell line was generated by stably integrating a fluorescent reporter cassette into the AAVS1 safe harbor locus of an HEK293T cell line (ATCC, CRL-3216). The shaker reporter cassette was designed so that when integrated into the genome, constitutively active expression of a shaker reporter gene is produced. The shaker reporter gene consists of an mCherry gene fused to an eGFP gene, linked together by a described shaker mutant Myo7a exon 18 (nucleotide c.2158C>T; amino acid Q720X). (Gibson et al, 1995) The construct is designed so that, by default, translation of the reporter gene message is terminated by the disease-causing nonsense mutation from the shaker-1 Myo7a gene, resulting in translation of only the mCherry protein. When the nonsense mutation is “repaired” (c.2158T>C), the corresponding stop codon changes to that wildtype Myo7a gene (amino acid X720Q). Successful repair of the mutant shaker-1 exon results in the expression of a dually fluorescent multimer composed of mCherry and eGFP proteins, linked together by a repaired Myo7a exon. The readout for successful correction of the shaker1 mutation in this model is therefore represented by both green (480-520nm) and red (600-640nm) fluorescence.

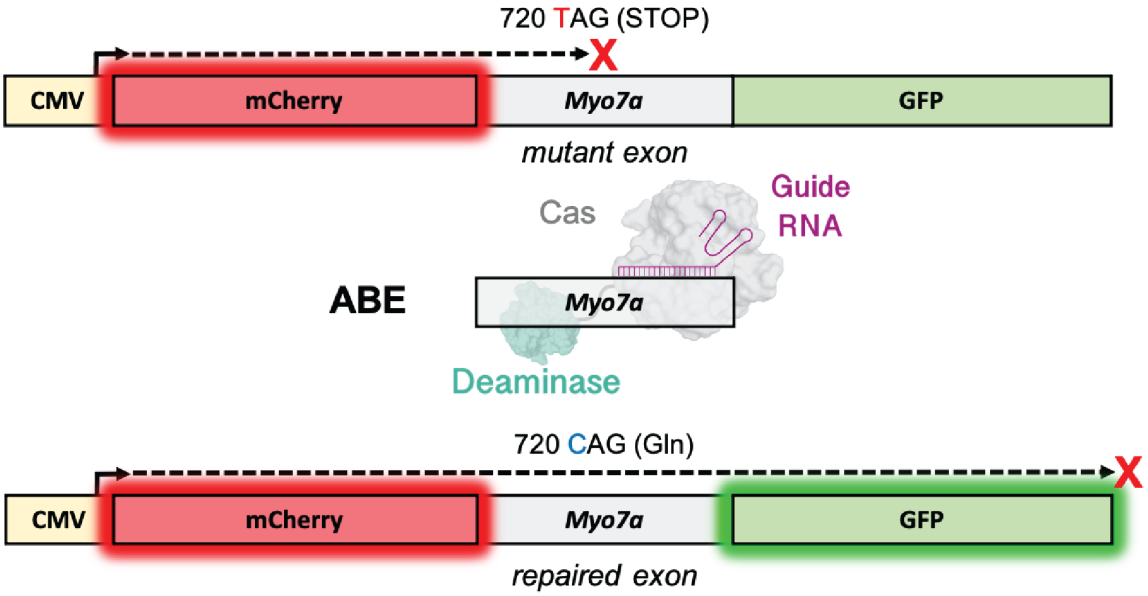

Figure 5: Schematic illustrating the 293T Shaker reporter system and the general approach for screening base editor guides. When integrated, mCherry is constitutively expressed by default. Translation of the gene is terminated by the premature stop codon in the mutant exon. Conversion of the disease-causing mutation from thymine to cystine results in expression of a dually fluorescent protein.

Model Validation

To validate this model, cultures were tested using a Cas9 adenine base editor (ABE) system. Two potential guide RNA sequences (gRNA1 and gRNA2) were selected according to the available PAM sequences (NG) surrounding the shaker-1 mutation, and guide RNA expressing vectors were cloned. Base editor and gRNA vectors were co-transfected into cultured 293T shaker reporter cells, and then analyzed 72 hours later by fluorescent microscopy, western blot, and fluorescence-activated cell aborting (FACS) (Figure 6).

Samples transfected with base editor vector alone, and no guide RNA vector, had no increase in green fluorescence. Samples transfected with base editor and guide RNA vectors (gRNA1 or gRNA2) showed significant green fluorescence, indicating successful correction of the shaker-1 mutation in these cells (Fig.6A). An approximate gene correction efficiency of each

guide was calculated by FACS analysis, 55% for gRNA1 and 52% for gRNA2 (Fig 6B). Expression of the mCherry-shaker_exon-eGFP protein was confirmed by western blot analysis of these samples (Fig. 6C). Sanger sequencing confirmed that in each sample, the disease-causing mutation was repaired (Fig 6D). Guide RNA 2 produced additional “off-target” modifications to the Myo7a gene, resulting in the introduction of a missense mutation (c.2162T>C; p.I721T).

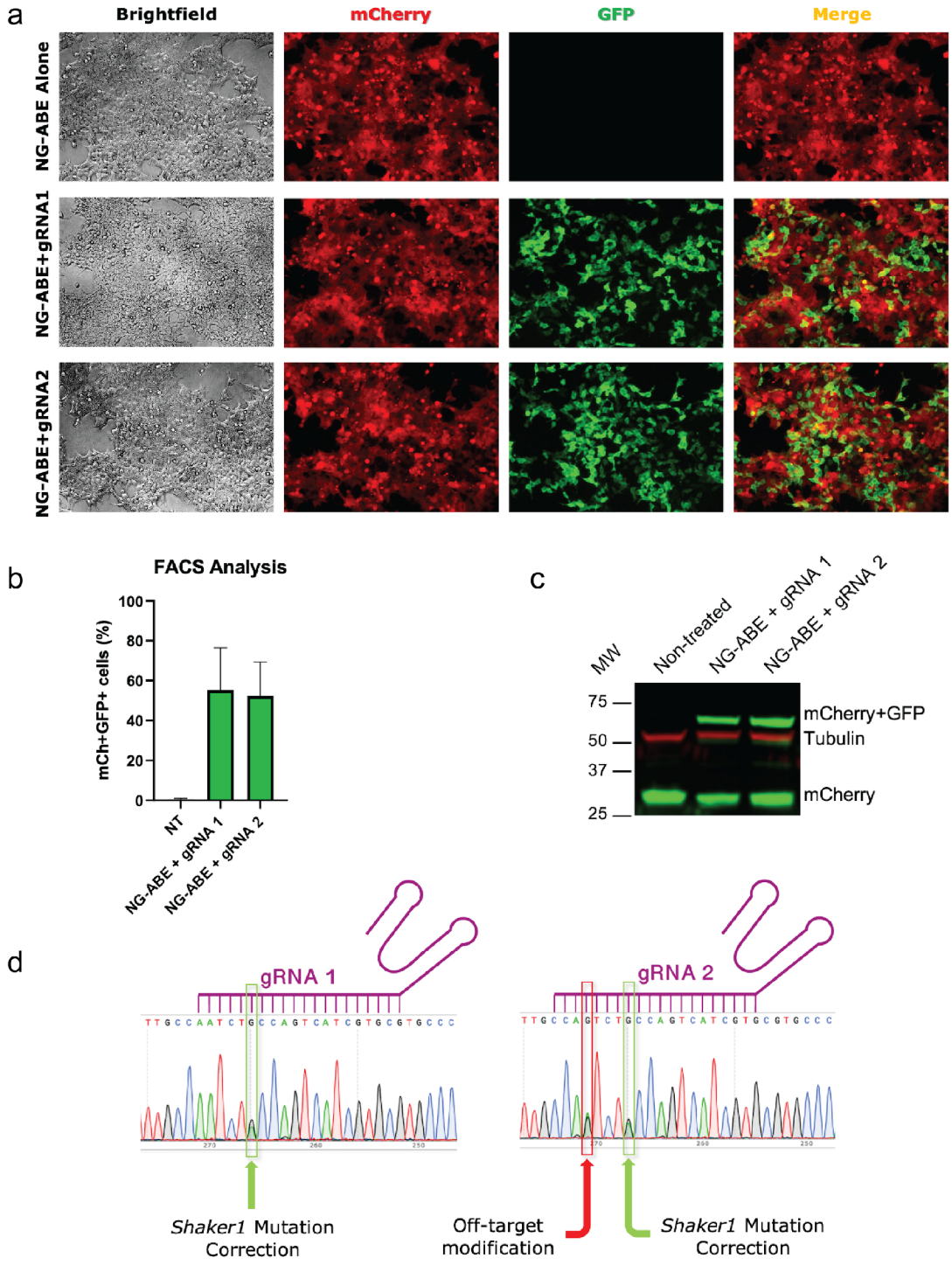

Figure 6: Validation of 293T reporter cell line and NG-ABE8e guides. A) Fluorescent images of 293T shaker reporters treated with base editor with or without guides. B) FACS plot of treated samples quantifying editing efficiency of each treatment. C) Western blot analysis of treated groups blotting for mCherry and tubulin. D) Sanger sequencing results from treated samples highlighting edits caused by corresponding guides.

To validate this system using in living animal tissue, we transfected our guide and base editor vectors into shaker-1 primary RPE cultures ex vivo. Restoration of MYO7a protein expression was observed in both lipofected and nucleofected RPE samples (Figure 7B).

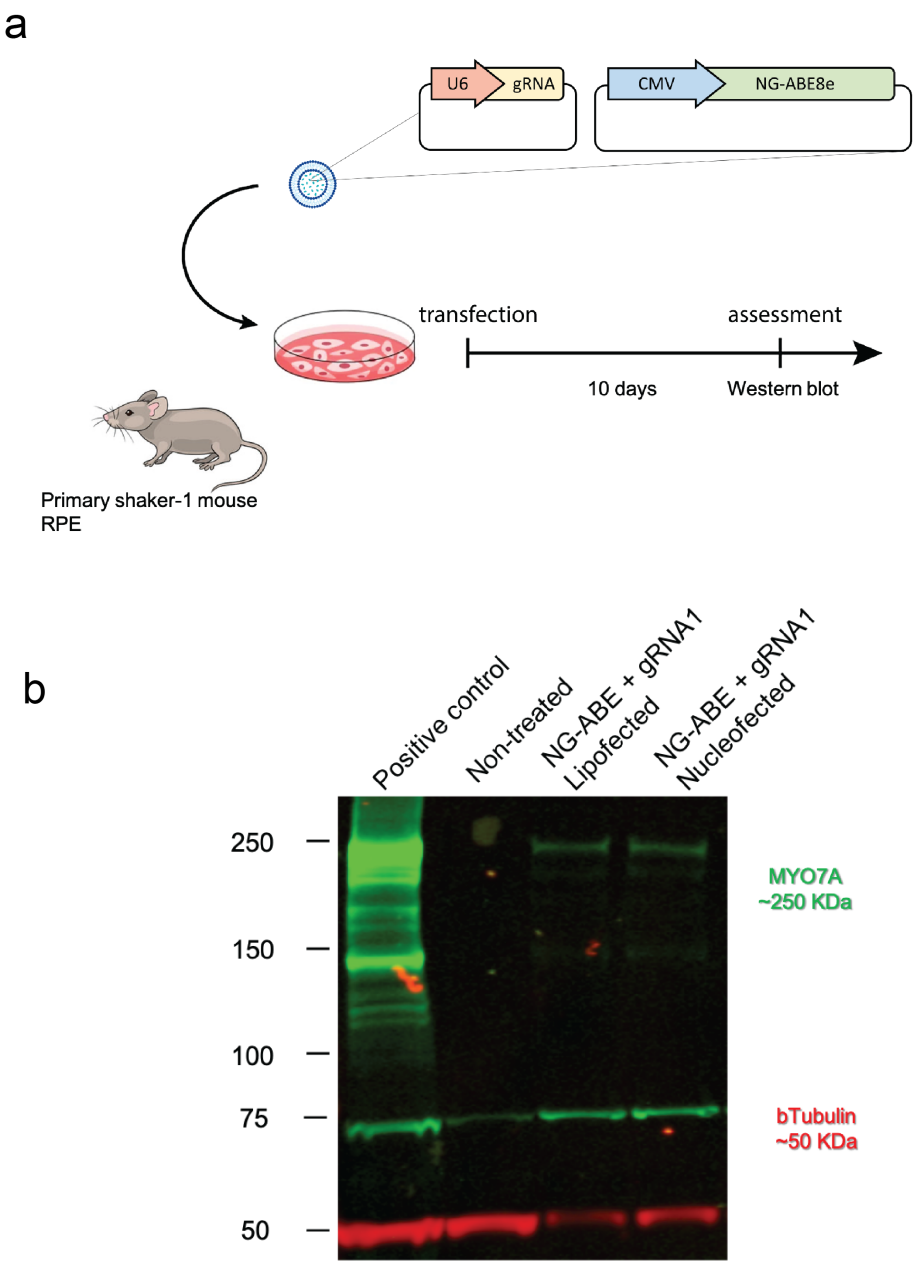

Figure 7: Validation of base editing system to rescue Myo7a in shaker-1 primary RPE. A) Schematic of experimental approach. B) Western blot of primary shaker-1 mouse RPE sample groups treated with base editors.

Vector Optimization

To improve our base editing system for in vivo translation, we required a smaller base editor gene construct that would allow us to consolidate the base editor and guide RNA genes into a single “all-in-one” vector system. For this we adopted the Nme2 adenine base editor (Nme2-ABE) and designed new guide sequences (gRNA3 and gRNA4) capable of targeting the shaker-1 mutation. We validated the Nme2-ABE and each guide by transfecting them in 293T reporter cells and observed a better editing efficiency with gRNA4 (Fig. 8A) Next, we consolidated the Nme2-ABE and gRNA genes into a single “all-in-one” vector, thereby reducing the number of delivery particles required for gene correction. As demonstrated by other studies, (Zhang et al., 2022) ABE editing efficiency is affected by the orientation of guide and base editor genes when combined into a single vector construct. Therefore, we generated two “all-in-one” Nme2-ABE-gRNA4 constructs by assembling the genes with promoters driving expression either in the same direction (“cis” orientation) or in opposite directions (“trans” orientation). We tested the relative editing efficiencies of these constructs by transfection into 293T shaker reporter cell cultures. Both vector orientations performed similarly, with “trans” orientation appearing to perform slightly better. (Fig. 8B) All base editor and guide combinations were then validated for functional gene rescue by western blot (Fig. 8C) , and editing efficiency was approximated by fluorescent cell counting. (Fig 8D)

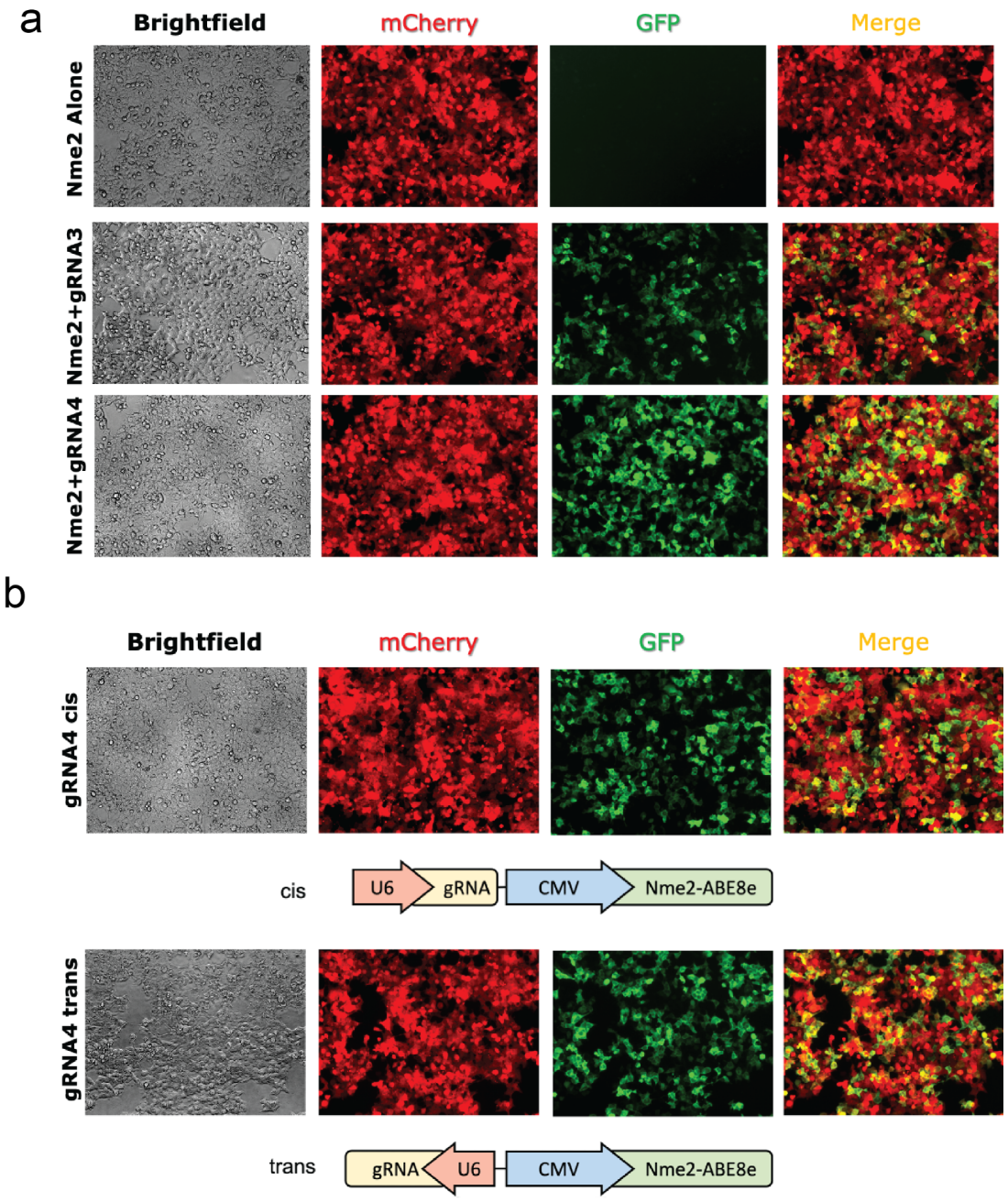
a
Brightfield
mCherry
GFP
Merge
Nme2 Alone
Nme2+gRNA3
Nme2+gRNA4
b
Brightfield
mCherry
GFP
Merge
gRNA4 cis
cis
U6
gRNA
CMV
Nme2-ABE8e
gRNA4 trans
trans
gRNA
U6
CMV
Nme2-ABE8e

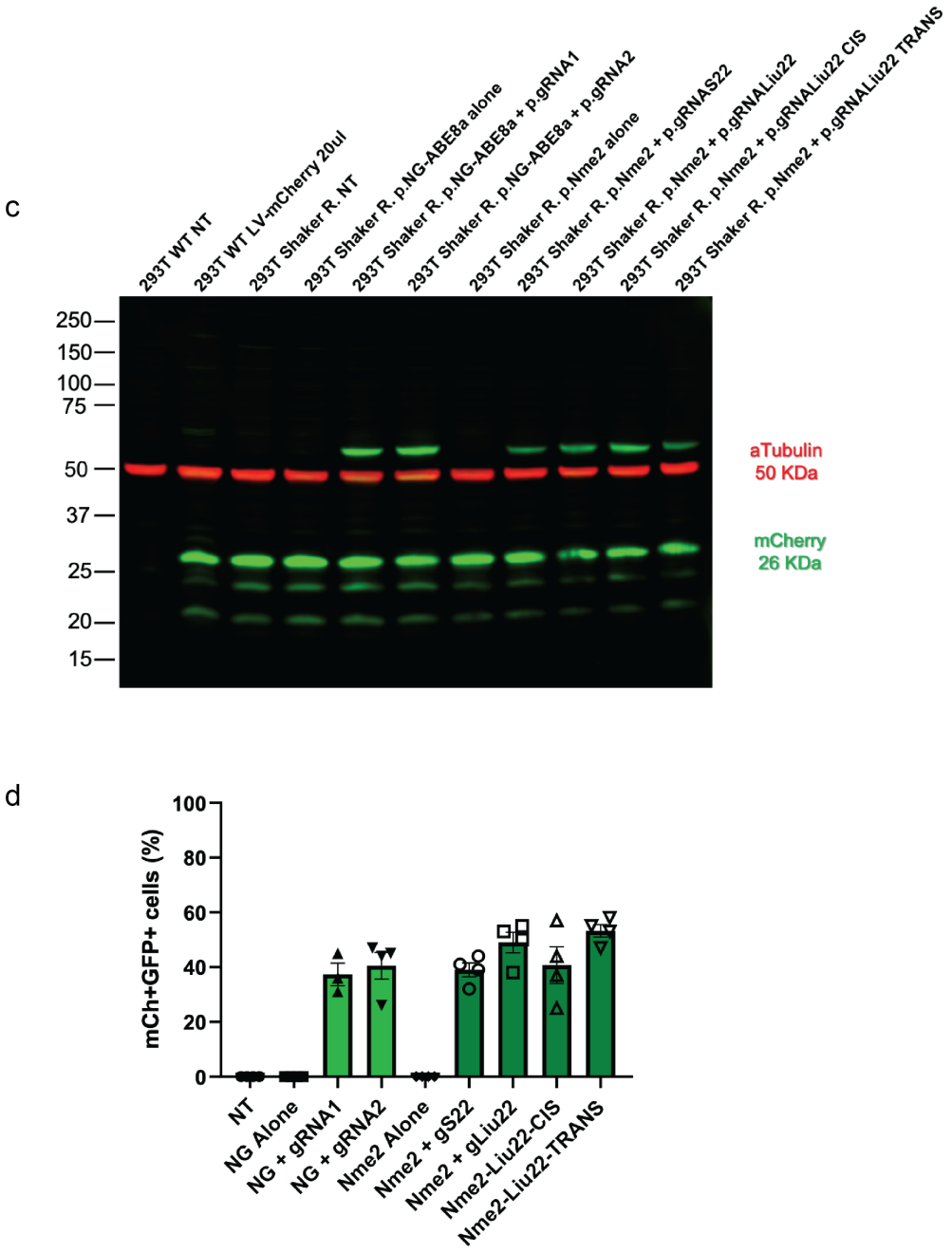

Figure 8: Validation of Nme2 adenine base editor and analysis of correction efficiencies in 293T shaker reporter cell line model using a dual vector approach. A) Fluorescent microscope images of samples treated with Nme2 with and without guides. B) Validation of Nme2-ABE-gRNA "all-in-one" constructs and comparison of gene orientation effects. C) Western blot analysis of each base editor and guide pair used so far. D) Quantification of editing efficiency approximated using fluorescent cell counting.

With an optimized vector system in-hand, we next adapted our system for in vivo testing. The Nme2-ABE-gRNA4 gene construct was cloned into a lentiviral vector (pUltraHot) backbone and then packaged into lentiviral particles using wildtype HEK293T cells. Lentivirus-containing media was filtered and concentrated in preparation for delivery into shaker-1 mouse retinas. Prepared lentivirus was injected into the subretinal space in one eye of two adult shaker-1 mice. After three or four weeks, shaker-1 retinas were dissected and analyzed. (Fig. 9) We assessed the correction of the mouse *Myo7a* gene by rescue of MYO7a protein expression in dissected retinal tissues. (Fig. 10) Failure of significant gene correction using our approach was demonstrated by the absence of MYO7a in our lentivirus-treated samples.

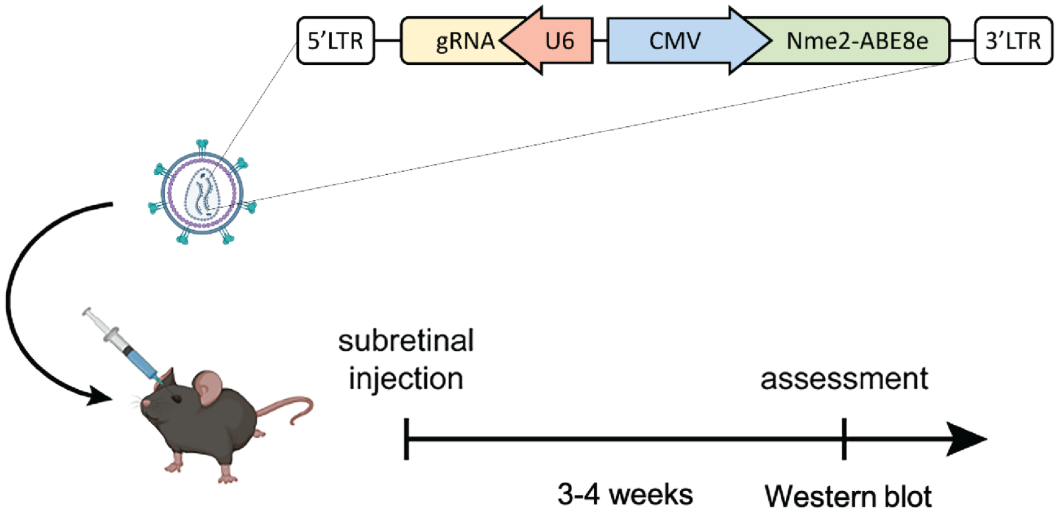

Figure 9: Schematic illustrating the approach used to validate the ABE8e-gRNA4 lentiviral vector in shaker-1 mice.

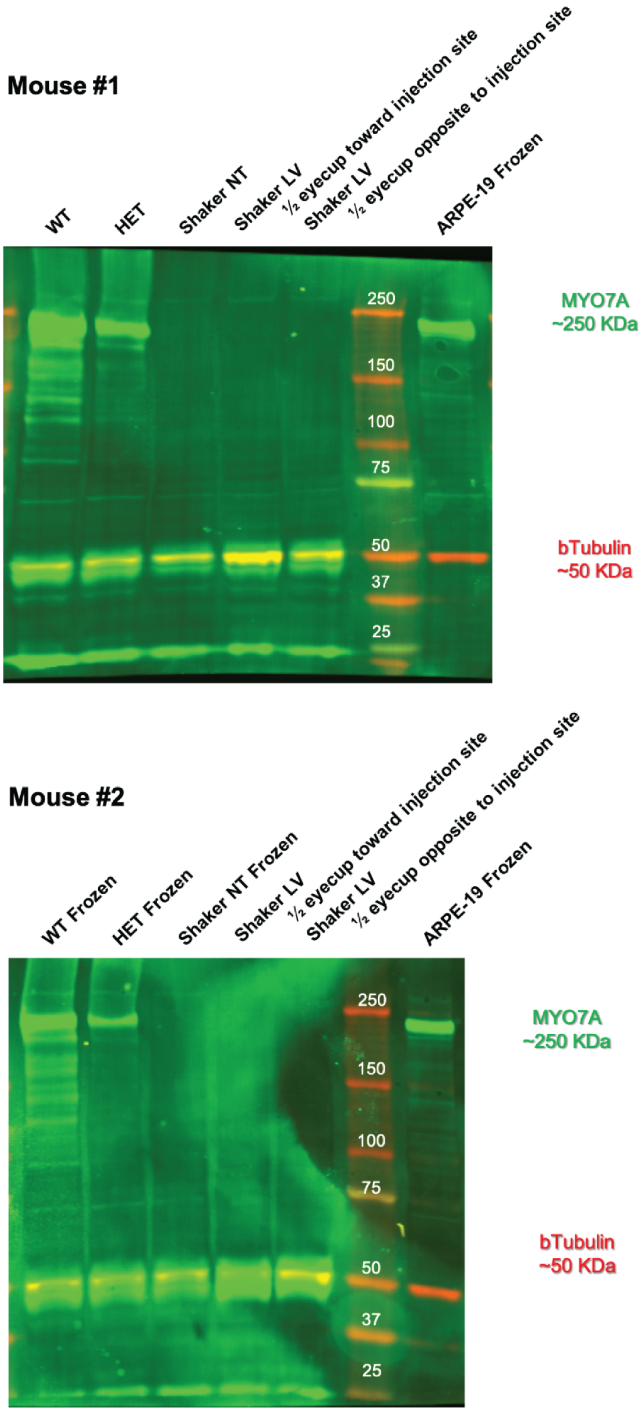

Figure 10: Western blot analysis of shaker-1 retina tissues treated with Nme2-gRNA4 lentivirus. Indication of Myosin VIIa protein rescue by a band approximately 250kDa in size was not observed in either mouse retina tested.

Methods

293T Shaker Reporter Line Development

The reporter cassette was constructed through a 2-step cloning process. First, an mCherry gene, a mutant shaker-1 exon (Myo7a exon 18; Myo7a cDNA nucleotides 2095–2191, from Shaker-1 mouse fibroblast cDNA), and an eGFP gene were PCR amplified and assembled into a KpnI-digested pCMV-bGHpolyA backbone plasmid. From this construct, the CMV-mCherry-shaker_exon-eGFP-bGHpA was PCR amplified (Platinum SuperFi PCR Master Mix, ThermoFisher) and ligated into a SalI restriction digested AAVS SA-2A-puro-pA donor plasmid (Plasmid #22075, Addgene). Both of these steps were performed using Gibson assembly (NEBuilder DNA Assembly Master Mix, NEB). The completed vector is referred to as the "AAVS1 shaker reporter donor vector." Genomic integration of this vector by homologous recombination into HEK293T cells was achieved by co-transfection (Lipofectamine 3000, Invitrogen) of the AAVS1 shaker reporter donor vector and a pair of TALEN vectors targeting the AAVS1 locus. TALEN vectors were provided by the Reza Ardehali Cardiology Research Laboratory at UCLA. Transfected HEK293T cells were cultured with 1µg/mL puromycin from 72 hours post-transfection to select for cells with the integrated reporter vector. Successful integration of the donor vector was signified by stable red fluorescence, as indicated by constitutive mCherry expression by each cell.

AAVS1 Shaker Reporter Construct Cloning

The reporter cassette was constructed through a 2-step cloning process. Both steps were performed using Gibson assembly (NEBuilder DNA Assembly Master Mix, NEB). First, an

mCherry gene, a mutant shaker-1 exon (Myo7a exon 18; Myo7a cDNA nucleotides 2095–2191, from Shaker-1 mouse fibroblast cDNA), and an eGFP gene were PCR amplified (Platinum SuperFi PCR Master Mix, ThermoFisher; Primer sequences listed in Table#) and assembled into a KpnI-digested pCMV-bGHpolyA backbone plasmid. From this construct, the CMV-mCherry-shaker_exon-eGFP-bGHpA was PCR amplified and assembled into a SalI restriction digested AAVS SA-2A-puro-pA donor plasmid (Plasmid #22075, Addgene). Genomic integration of this vector by homologous recombination into HEK293T cells was achieved by co-transfection (Lipofectamine 3000, Invitrogen) of the AAVS1 shaker reporter donor vector and a pair of TALEN vectors targeting the AAVS1 locus. TALEN vectors were provided by the Reza Ardehali Cardiology Research Laboratory at UCLA.

pX552 Guide RNA Vector Cloning

Single-stranded DNA oligonucleotides containing guide RNA sequences with overhanging adapter sequences were designed according to previously described methods. (Zhang et al, 2014) Each oligo pair was annealed, phosphorylated (Recombinant Shrimp Alkaline Phosphatase, NEB), and then ligated (Quick Ligation Kit, NEB) into a BsaI digested pX552 backbone vector. (Addgene plasmid #60958) Ligation reactions were transformed into competent bacteria cells and plated onto LB-Ampicillin selection plates. Purified plasmid DNA was extracted from expanded clonal bacteria cultures (Purelink HiPure Midiprep Kit, Invitrogen).

Table 3: pX552 Guide RNA primers

Primer Name	Sequence
Shaker ABE gRNA t1A	CACCGAATCTACCAGTCATCGTGCG
Shaker ABE gRNA t1B	AAACCGCACGATGACTGGTAGATTC
Shaker ABE gRNA t2A	CACCGCCAATCTACCAGTCATCGTG
Shaker ABE gRNA t2B	AAACCCAATCTACCAGTCATCGTGC

Table 4: Nme2 Guide RNA primers

Primer Name	Sequence
Nme gRNA clone R	GGTGTTTCGTCCTTTCCACAAG
Nme gRNA3 clone F	GCCAATCTACCAGTCATCGTGGTTGTAGCTCCCTTTCTCATTTCG
Nme gRNA3 clone R	GTGCCAATCTACCAGTCATCGTGGTTGTAGCTCCCTTTCTCATTTCG
Nme gRNA4 clone F	GCAATCTACCAGTCATCGTGCGTTGTAGCTCCCTTTCTCATTTCG
Nme gRNA4 clone F	GGCCAATCTACCAGTCATCGTGCGTTGTAGCTCCCTTTCTCATTTCG

Western Blot

Cultured 293T shaker reporter cells were harvested 4-6 days post-transfection. Protein lysate samples were extracted from cells (Protein extraction) and run on a polyacrylamide gel (NuPAGE 4 to 12% Bis-Tris, Invitrogen) at 100V for approximately 1 hour. Gel-suspended protein was transferred onto a nitrocellulose membrane on ice. Membranes were blotted with anti-tubulin and anti-MYO7A antibodies.

Cell counting

293T shaker reporter cells were harvested at least 48 hours following ABE and gRNA vector transfection. Culture media was removed from each well, and replaced with 0.25% trypsin (ThermoFisher). Cells were then incubated for approximately 5 minutes in the tissue culture incubator. Next, trypsin was deactivated by adding 3 volumes of D10 media, and cells were centrifuged for 5 minutes at 1000RPM. Supernatant was removed, and the cell pellet was resuspended in an appropriate volume of D10 media. 10µL of the cell suspension was ejected into a cell counter plate, and analyzed using the cell counter (ThermoFisher).

DISCUSSION

Gene Augmentation Therapy for USH1B

Heterogeneity in disease-causing mutations along *MYO7A* make gene augmentation a rational approach to gene therapy, as one treatment could theoretically be used to treat any USH1B patient. Delivery of full-length *MYO7A* for the treatment of USH1B presents a unique set of challenges for the field of retinal gene therapy. The relatively large cDNA size of *MYO7A* (6.6kb) means that packaging efficiency is an issue for certain vectors, and therefore choosing the proper delivery vehicle is a critical step for developing a vector capable of gene transfer. The majority of work within the field has focused on optimizing lentiviral or AAV vectors to address this.

Pioneering studies of USH1B gene therapy demonstrated that lentiviral-mediated gene transfer of human *MYO7A* to a *Myo7a*-deficient mouse retina successfully rescues some disease associated phenotypes in the RPE and photoreceptors. (Hashimoto et al., 2007) Considering the large cDNA size of *MYO7A* (6.6kb), large capacity viruses, such as lentiviruses, make reasonable vectors for packaging. An alternative lentiviral vector derived from equine infectious anaemia virus (EIAV) has been proposed for therapeutic gene transfer of human *MYO7A*. (Zallochi et al., 2014) Subretinal delivery of this vector demonstrated some efficacy in protecting shaker1 mouse retinas from light-induced degeneration, and was well-tolerated in non-human primates. This vector would later be used for the clinical treatment of USH1B RD under the name UshStat. (Zallochi et al., 2014). Though promising in their potential, lentiviral

vectors do have their limitations. As discussed previously, they are randomly integrating vectors, and so genotoxicity is a risk factor when administered.

AAVs are another viral vector used for therapeutic transgene delivery of *MYO7A*. Compared to other viral vectors, they generally have superior gene expression stability and tissue specificity with very low immunogenicity. Efficient targeting of AAVs to the RPE and photoreceptor cells has been repeatedly demonstrated. (Ail et al., 2023) The primary concern with using AAVs to package *MYO7A* for augmentation therapy is the limited packaging capacity (4.7kb). (Wu et al., 2010; Salganik et al., 2015) To address this, a dual vector delivery approach is possible, in which the vector construct (including the large *MYO7A* coding gene) must be split into separate AAV vectors. When co-delivered to target cells, the two construct sections recombine into one fully intact gene construct. Viability of this approach has been demonstrated for delivery of several different large gene constructs to an animal retina, including *MYO7A (*Alloca et al., 2008; Colella et al., 2014), however questions still remain regarding the sufficiency of this approach to alleviate disease in human subjects. Recent studies using the dual-AAV approach to rescue hearing loss in an USH1B mouse model does boost optimism for USH1B gene augmentation therapy. (Lau et al., 2023) AAV delivery of base editing to the retina for gene repair in the retina has been demonstrated (Choi et al., 2022), suggesting that this approach may be suitable for USH1B gene therapy.

An additional consideration for gene augmentation is the stability of gene expression in treated tissues. Toxicity of *MYO7A* overexpression has been reported. (Hashimoto et al, 2007) This indicates that potential issues with gene regulation could pose additional challenges in the development of viable gene augmentation therapies. This issue is not unique to treating

USH1B, as many groups have addressed this by developing vector systems that use gene-specific promoters and regulatory elements in order to fine-tune gene expression in treated tissues. Some of this work is currently underway for the development of gene augmentation approaches for diseases like Duschene muscular dystrophy (Meng et al., 2022) and X-linked chronic granulomatous disease (X-CGD). (Wong et al., 2023)

CRISPR, Base Editing, and the Future

The year 2023 marks the 10-year anniversary since the discovery of CRISPR/Cas9 as a convenient approach for modifying genetic information in a living system. Over the last decade, CRISPR technology has rapidly evolved into a suite of powerful tools for studying how genes work and how we can manipulate them for the betterment of mankind. These tools have ushered in a new age of scientific research and therapeutic techniques for treating disease. In December 2023, the first ever CRISPR-Cas-based therapy was approved by the United States FDA. In just over a decade, we are witnessing a biomedical revolution from the conception of a single tool. Our work is one such demonstration of the power of CRISPR technology. We have demonstrated one potential application of the CRISPR base editing system for treating USH1B, a devastating disease thought to have no cure in sight. Though this system may still not be an appropriate treatment approach for USH1B-associated blindness in its current form, the insights we gain from our exploration of the tools inspires the future of gene editing as a potential therapeutic approach for inherited genetic diseases.

Closing Remarks

In Chapter 1, we demonstrated that the two major isoforms of the *MYO7A* gene are expressed in the retina. The expression of both isoforms is conserved across species, inferring that both forms may be critical for normal gene function. In Chapter 2, we developed a set of tools that can be used to study these different isoforms in order to better understand their roles in the tissues of the retina. These tools can be used to study the role of *MYO7A* in other systems as well, including tissues that express *MYO7A* but do not show signs of disease described in USH1B patients. Finally, in Chapter 3, we demonstrated the potential of CRISPR base editors for correcting disease-causing mutations in the Myo7a gene. We also developed a simple, high-throughput cell culture model for screening through guide RNAs to a shaker1 nonsense mutation. This approach can be further developed to explore editing of other potentially harmful nonsense mutations by simply swapping the shaker1 sequence with other disease gene sequences. Together, this work has advanced the understanding of *MYO7A* in the retina, provided novel tools for further exploring the functions of the gene, and provided hope of a cure for USH1B.

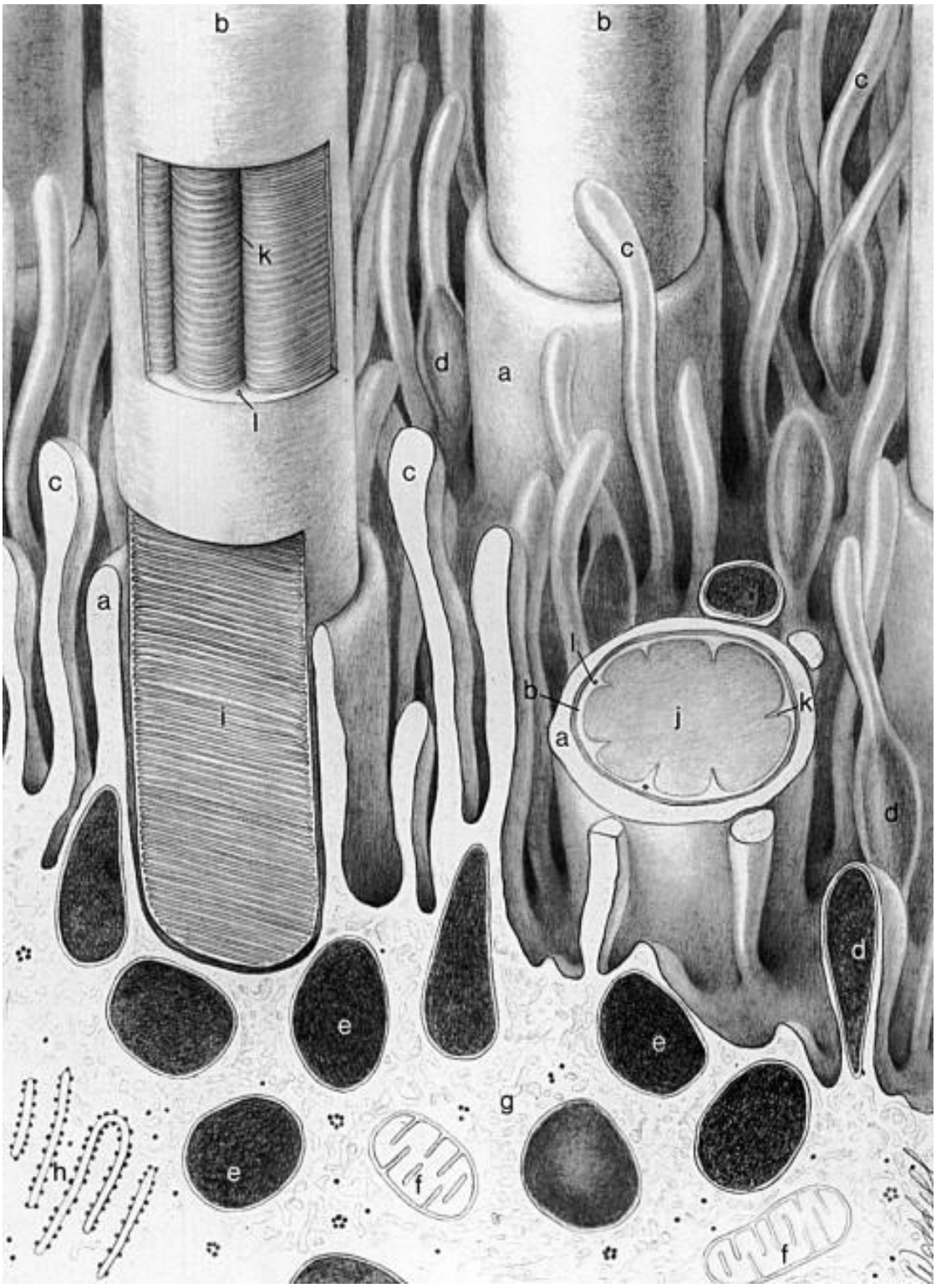

Figure 11: 3-D illustration of RPE and photoreceptor outer segments interfacing at the subretinal space.
Adapted from Remington, 2012.

Appendix

Table 5: Important functional domains and their corresponding amino acid and nucleotide numbers, according to the *MYO7A* Isoform 1 coding region

Amino Acids	Corresponding Nucleotides	Functional Domain
60-741	180-2223	Motor Domain / Large ATPases
766-787	2298-2361	IQ Calmodulin-binding motif
965-1604	2895-4812	MF1 (MyTH4-FERM1)
1605-1669	4815-5007	Src homology 3 (SH3) domain
1763-2206	5289-5688	MF2 (MyTH4-FERM2)

Table 6: Gene Vector Element Properties

	Gene Size	Protein Size
Coding Genes		
MYO7A IF1:	6642 bp	254 kDa
MYO7A IF2:	6528 bp	250 kDa
mCh-*MYO*7A IF1	7397 bp	282 kDa
mCh-*MYO7A* IF2	7284 bp	278 kDa
spCas9:	4104 bp	162 kDa
NG ABE-Cas9:	4818 bp	184 kDa
Nme2 Cas9:	3252 bp	125 kDa
Nme2 ABE8e-Cas9:	3957 bp	182 kDa
Promoters		
EFS:	212 bp	
U6:	241 bp	
U6 mini:	112 bp	
CMV:	584 bp	
U1a:	251 bp	
Additional elements		
ß-globin pA:	56 bp	
WPRE:	589 bp	
Nucleoplasmin NLS	48 bp	
SV40 NLS	21 bp	
Complete Vectors		

CMV-Nme2ABE8e-pA	4893bp
CMV-Nme2ABE8e-pA + U6-gRNA	5355bp

References:

Remington, L. A. (2012). Retina. In *Clinical Anatomy and Physiology of the Visual System* (pp. 61–92). Elsevier. https://doi.org/10.1016/B978-1-4377-1926-0.10004-9
Kimbrel, E. A., & Lanza, R. (2020). Retinal degeneration. In *Principles of Tissue Engineering* (pp. 1145–1162). Elsevier. https://doi.org/10.1016/B978-0-12-818422-6.00064-2

Ruiz, F., Pinilla, I., Cuenca, N., Vidal-Sanz, M., Villegas-Pérez, M. P., & Agudo-Barriuso, M. (2020). Tracing the retina to analyze the integrity and phagocytic capacity of the retinal pigment epithelium. *Scientific Reports*, *10*(1), 7273. https://doi.org/10.1038/s41598-020-64131-z

McKay, B. S. (2019). Pigmentation and vision: Is GPR143 in control? *Journal of Neuroscience Research*, *97*(1), 77–87. https://doi.org/10.1002/jnr.24246

Storm, T., Burgoyne, T., & Futter, C. E. (2020). Membrane trafficking in the retinal pigment epithelium at a glance. *Journal of Cell Science*, *133*(16), jcs238279. https://doi.org/10.1242/jcs.238279

El-Amraoui, A., Schonn, J., Küssel-Andermann, P., Blanchard, S., Desnos, C., Henry, J., Wolfrum, U., Darchen, F., & Petit, C. (2002). MyRIP, a novel Rab effector, enables myosin VIIa recruitment to retinal melanosomes. *EMBO Reports*, *3*(5), 463–470. https://doi.org/10.1093/embo-reports/kvf090

Futter, C. E., Ramalho, J. S., Jaissle, G. B., Seeliger, M. W., & Seabra, M. C. (2004). The Role of Rab27a in the Regulation of Melanosome Distribution within Retinal Pigment Epithelial Cells. *Molecular Biology of the Cell*, *15*(5), 2264–2275. https://doi.org/10.1091/mbc.e03-10-0772

Gibbs, D., Azarian, S. M., Lillo, C., Kitamoto, J., Klomp, A. E., Steel, K. P., Libby, R. T., & Williams, D. S. (2004). Role of myosin VIIa and Rab27a in the motility and localization of RPE melanosomes. *Journal of Cell Science*, *117*(26), 6473–6483. https://doi.org/10.1242/jcs.01580

Lopes, V. S., Ramalho, J. S., Owen, D. M., Karl, M. O., Strauss, O., Futter, C. E., & Seabra, M. C. (2007). The Ternary Rab27a–Myrip–Myosin VIIa Complex Regulates Melanosome Motility in the Retinal Pigment Epithelium. *Traffic*, *8*(5), 486–499. https://doi.org/10.1111/j.1600-0854.2007.00548.x

Zhang, Q.-X., Lu, R.-W., Messinger, J. D., Curcio, C. A., Guarcello, V., & Yao, X.-C. (2013). In vivo Optical Coherence Tomography of Light-Driven Melanosome Translocation in Retinal Pigment Epithelium. *Scientific Reports*, *3*(1), 2644. https://doi.org/10.1038/srep02644

Mazzoni, F., Safa, H., & Finnemann, S. C. (2014). Understanding photoreceptor outer segment phagocytosis: Use and utility of RPE cells in culture. *Experimental Eye Research*, *126*, 51–60. https://doi.org/10.1016/j.exer.2014.01.010

Young, R. W., & Bok, D. (1969). Participation of the Retinal Pigment Epithelium In The Rod Outer Segment Renewal Process. *The Journal of Cell Biology*, *42*(2), 392–403. https://doi.org/10.1083/jcb.42.2.392

Young, R. W. (1977). The daily rhythm of shedding and degradation of cone outer segment membranes in the lizard retina. *Journal of Ultrastructure Research*, *61*(2), 172–185. https://doi.org/10.1016/S0022-5320(77)80084-1

Goldman, A. I., & Teirstein, P. S. (1980). The role of ambient lighting in circadian disc shedding in the rod outer segment of the rat retina. *Investigative ophthalmology & visual science*, *19*(11), 1257–1267.

LaVail, M. M. (1980). Circadian nature of rod outer segment disc shedding in the rat. *Investigative ophthalmology & visual science*, *19*(4), 407–411.

Kocaoglu, O. P., Liu, Z., Zhang, F., Kurokawa, K., Jonnal, R. S., & Miller, D. T. (2016). Photoreceptor disc shedding in the living human eye. *Biomedical Optics Express*, *7*(11), 4554. https://doi.org/10.1364/BOE.7.004554

Kennedy, C. J., Rakoczy, P. E., & Constable, I. J. (1995). Lipofuscin of the retinal pigment epithelium: A review. *Eye*, *9*(6), 763–771. https://doi.org/10.1038/eye.1995.192

Feng, W., Yasumura, D., Matthes, M. T., LaVail, M. M., & Vollrath, D. (2002). Mertk Triggers Uptake of Photoreceptor Outer Segments during Phagocytosis by Cultured Retinal Pigment Epithelial Cells. *Journal of Biological Chemistry*, *277*(19), 17016–17022. https://doi.org/10.1074/jbc.M107876200

Mullen, R. J., M. M. LaVail. (1976). Inherited Retinal Dystrophy: Primary Defect in Pigment Epithelium Determined with Experimental Rat Chimeras.*Science*192,799-801. https://doi.org/10.1126/science.1265483

Burstyn-Cohen, T., Lew, E. D., Través, P. G., Burrola, P. G., Hash, J. C., & Lemke, G. (2012). Genetic Dissection of TAM Receptor-Ligand Interaction in Retinal Pigment Epithelial Cell Phagocytosis. *Neuron*, *76*(6), 1123–1132. https://doi.org/10.1016/j.neuron.2012.10.015

Nandrot, E. F., Kim, Y., Brodie, S. E., Huang, X., Sheppard, D., & Finnemann, S. C. (2004). Loss of Synchronized Retinal Phagocytosis and Age-related Blindness in Mice Lacking αvβ5 Integrin. *The Journal of Experimental Medicine*, *200*(12), 1539–1545. https://doi.org/10.1084/jem.20041447

Nandrot, E. F., Anand, M., Almeida, D., Atabai, K., Sheppard, D., & Finnemann, S. C. (2007). Essential role for MFG-E8 as ligand for αvβ5 integrin in diurnal retinal phagocytosis. *Proceedings of the National Academy of Sciences*, *104*(29), 12005–12010. https://doi.org/10.1073/pnas.0704756104

Gordon, W. C., De Turco, E. B. R., & Bazan, N. G. (1992). Retinal pigment epithelial cells play a central role in the conservation of docosahexaenoic acid by photoreceptor cells after shedding and phagocytosis. *Current Eye Research*, *11*(1), 73–83. https://doi.org/10.3109/02713689209069169

Thompson, D. A., & Gal, A. (2003). Vitamin A metabolism in the retinal pigment epithelium: Genes, mutations, and diseases. *Progress in Retinal and Eye Research*, *22*(5), 683–703. https://doi.org/10.1016/S1350-9462(03)00051-X

Baehr, W., Wu, S. M., Bird, A. C., & Palczewski, K. (2003). The retinoid cycle and retina disease. *Vision Research*, *43*(28), 2957–2958. https://doi.org/10.1016/j.visres.2003.10.001

Blaauwgeers, H. G. T., Holtkamp, G. M., Rutten, H., Witmer, A. N., Koolwijk, P., Partanen, T. A., Alitalo, K., Kroon, M. E., Kijlstra, A., Van Hinsbergh, V. W. M., & Schlingemann, R. O. (1999). Polarized Vascular Endothelial Growth Factor Secretion by Human Retinal Pigment Epithelium and Localization of Vascular Endothelial Growth Factor Receptors on the Inner Choriocapillaris. *The American Journal of Pathology*, *155*(2), 421–428. https://doi.org/10.1016/S0002-9440(10)65138-3

Roberts, W. G., & Palade, G. E. (1995). *Increased microvascular permeability and endothelial fenestration induced by vascular endothelial growth factor*. *Journal of cell science*, *108 (Pt 6)*, 2369–2379. https://doi.org/10.1242/jcs.108.6.2369

Padgett, L. C., Lui, G.-M., Werb, Z., & Lavail, M. M. (1997). Matrix Metalloproteinase-2 and Tissue Inhibitor of Metalloproteinase-1 in the Retinal Pigment Epithelium and

Interphotoreceptor Matrix: Vectorial Secretion and Regulation. *Experimental Eye Research*, *64*(6), 927–938. https://doi.org/10.1006/exer.1997.0287

Cao, W., Wen, R., Li, F., Lavail, M. M., & Steinberg, R. H. (1997). Mechanical Injury Increases bFGF and CNTF mRNA Expression in the Mouse Retina. *Experimental Eye Research*, *65*(2), 241–248. https://doi.org/10.1006/exer.1997.0328

Henderson, R. H. (2020). Inherited retinal dystrophies. *Paediatrics and Child Health*, *30*(1), 19–27. https://doi.org/10.1016/j.paed.2019.10.004

Suppiej, A., Marino, S., Reffo, M. E., Maritan, V., Vitaliti, G., Mailo, J., & Falsaperla, R. (2019). Early onset retinal dystrophies: Clinical clues to diagnosis for pediatricians. *Italian Journal of Pediatrics*, *45*(1), 168. https://doi.org/10.1186/s13052-019-0760-5

Prokofyeva, E., & Zrenner, E. (2012). Epidemiology of Major Eye Diseases Leading to Blindness in Europe: A Literature Review. *Ophthalmic Research*, *47*(4), 171–188. https://doi.org/10.1159/000329603

Georgiou, M., Fujinami, K., & Michaelides, M. (2020). Retinal imaging in inherited retinal diseases. *Annals of Eye Science*, *5*, 25–25. https://doi.org/10.21037/aes-20-81

Cross, N., Van Steen, C., Zegaoui, Y., Satherley, A., & Angelillo, L. (2022). Current and Future Treatment of Retinitis Pigmentosa. *Clinical Ophthalmology*, *Volume 16*, 2909–2921. https://doi.org/10.2147/OPTH.S370032

Mandai, M., Watanabe, A., Kurimoto, Y., Hirami, Y., Morinaga, C., Daimon, T., Fujihara, M., Akimaru, H., Sakai, N., Shibata, Y., Terada, M., Nomiya, Y., Tanishima, S., Nakamura, M., Kamao, H., Sugita, S., Onishi, A., Ito, T., Fujita, K., … Takahashi, M. (2017). Autologous Induced Stem-Cell–Derived Retinal Cells for Macular Degeneration. *New England Journal of Medicine*, *376*(11), 1038–1046. https://doi.org/10.1056/NEJMoa1608368

Schwartz, S. D., Regillo, C. D., Lam, B. L., Eliott, D., Rosenfeld, P. J., Gregori, N. Z., Hubschman, J. P., Davis, J. L., Heilwell, G., Spirn, M., Maguire, J., Gay, R., Bateman, J., Ostrick, R. M., Morris, D., Vincent, M., Anglade, E., Del Priore, L. V., & Lanza, R. (2015). Human embryonic stem cell-derived retinal pigment epithelium in patients with age-related macular degeneration and Stargardt's macular dystrophy: follow-up of two open-label phase 1/2 studies. *Lancet (London, England)*, *385*(9967), 509–516. https://doi.org/10.1016/S0140-6736(14)61376-3

Da Cruz, L., Fynes, K., Georgiadis, O., Kerby, J., Luo, Y. H., Ahmado, A., Vernon, A., Daniels, J. T., Nommiste, B., Hasan, S. M., Gooljar, S. B., Carr, A.-J. F., Vugler, A., Ramsden, C. M., Bictash, M., Fenster, M., Steer, J., Harbinson, T., Wilbrey, A., … Coffey, P. J. (2018). Phase 1 clinical study of an embryonic stem cell–derived retinal pigment epithelium patch in age-related macular degeneration. *Nature Biotechnology*, *36*(4), 328–337. https://doi.org/10.1038/nbt.4114

Zein, W. M., Jeffrey, B. G., Wiley, H. E., Turriff, A. E., Tumminia, S. J., Tao, W., Bush, R. A., Marangoni, D., Wen, R., Wei, L. L., & Sieving, P. A. (n.d.). CNGB3-Achromatopsia Clinical Trial With CNTF: Diminished Rod Pathway Responses With No Evidence of Improvement in Cone Function. *Investigative ophthalmology & visual science*, *55*(10), 6301–6308. https://doi.org/10.1167/iovs.14-14860

Collin, R. W., Den Hollander, A. I., Van Der Velde-Visser, S. D., Bennicelli, J., Bennett, J., & Cremers, F. P. (2012). Antisense Oligonucleotide (AON)-based Therapy for Leber Congenital Amaurosis Caused by a Frequent Mutation in CEP290. *Molecular Therapy - Nucleic Acids*, *1*, e14. https://doi.org/10.1038/mtna.2012.3

Gerard, X., Perrault, I., Hanein, S., Silva, E., Bigot, K., Defoort-Delhemmes, S., Rio, M., Munnich, A., Scherman, D., Kaplan, J., Kichler, A., & Rozet, J.-M. (2012). AON-mediated Exon Skipping Restores Ciliation in Fibroblasts Harboring the Common Leber Congenital Amaurosis CEP290 Mutation. *Molecular Therapy - Nucleic Acids*, *1*, e29. https://doi.org/10.1038/mtna.2012.21

Slijkerman, R. W., Vaché, C., Dona, M., García-García, G., Claustres, M., Hetterschijt, L., Peters, T. A., Hartel, B. P., Pennings, R. J., Millan, J. M., Aller, E., Garanto, A., Collin, R. W., Kremer, H., Roux, A.-F., & Van Wijk, E. (2016). Antisense Oligonucleotide-based Splice Correction for USH2A-associated Retinal Degeneration Caused by a Frequent Deep-intronic Mutation. *Molecular Therapy - Nucleic Acids*, *5*, e381. https://doi.org/10.1038/mtna.2016.89

Lentz, J. J., Jodelka, F. M., Hinrich, A. J., McCaffrey, K. E., Farris, H. E., Spalitta, M. J., Bazan, N. G., Duelli, D. M., Rigo, F., & Hastings, M. L. (2013). Rescue of hearing and vestibular function by antisense oligonucleotides in a mouse model of human deafness. *Nature Medicine*, *19*(3), 345–350. https://doi.org/10.1038/nm.3106

Mort, M., Ivanov, D., Cooper, D.N. and Chuzhanova, N.A. (2008), A meta-analysis of nonsense mutations causing human genetic disease. *Human Mutation*, 29: 1037-1047. https://doi.org/10.1002/humu.20763

Samanta, A., Stingl, K., Kohl, S., Ries, J., Linnert, J., & Nagel-Wolfrum, K. (2019). Ataluren for the Treatment of Usher Syndrome 2A Caused by Nonsense Mutations. *International Journal of Molecular Sciences*, *20*(24), 6274. https://doi.org/10.3390/ijms20246274

Moosajee, M., Gregory-Evans, K., Ellis, C. D., Seabra, M. C., & Gregory-Evans, C. Y. (2008). Translational bypass of nonsense mutations in zebrafish rep1, pax2.1 and lamb1 highlights a viable therapeutic option for untreatable genetic eye disease. *Human Molecular Genetics*, *17*(24), 3987–4000. https://doi.org/10.1093/hmg/ddn302

Goldmann, T., Overlack, N., Möller, F., Belakhov, V., Van Wyk, M., Baasov, T., Wolfrum, U., & Nagel-Wolfrum, K. (2012). A comparative evaluation of NB30, NB54 and PTC124 in translational read-through efficacy for treatment of an *USH1C* nonsense mutation. *EMBO Molecular Medicine*, *4*(11), 1186–1199. https://doi.org/10.1002/emmm.201201438

Lima Cunha, D., Sarkar, H., Eintracht, J., Harding, P., Zhou, J. H., & Moosajee, M. (2023). Restoration of functional PAX6 in aniridia patient iPSC-derived ocular tissue models using repurposed nonsense suppression drugs. *Molecular Therapy - Nucleic Acids*, *33*, 240–253. https://doi.org/10.1016/j.omtn.2023.06.016

Anderson, W. F., Blaese, R. M., & Culver, K. (1990). The ADA human gene therapy clinical protocol: Points to Consider response with clinical protocol, July 6, 1990. *Human gene therapy*, *1*(3), 331–362. https://doi.org/10.1089/hum.1990.1.3-331

Kohn, D. B., Mitsuya, H., Ballow, M., Selegue, J. E., Barankiewicz, J., Cohen, A., Gelfand, E., Anderson, W. F., & Blaese, R. M. (1989). Establishment and characterization of adenosine deaminase-deficient human T cell lines. *The Journal of Immunology*, *142*(11), 3971–3977. https://doi.org/10.4049/jimmunol.142.11.3971

Smithies, O., Gregg, R., Boggs, S. Koralewski, M. A., & Kucherlapati, R. S. (1985). Insertion of DNA sequences into the human chromosomal *β*-globin locus by homologous recombination. *Nature* 317, 230–234. https://doi.org/10.1038/317230a0

Smithies, O., Koralewski, M. A., Song, K.-Y., & Kucherlapati, R. S. (1984). Homologous Recombination with DNA Introduced into Mammalian Cells. Cold Spring Harb Symp Quant Biol 1984. 49: 161-170. https://doi.org/10.1101/SQB.1984.049.01.019

Kucherlapati, R. S., Eves, E. M., Song, K. Y., Morse, B. S., & Smithies, O. (1984). Homologous recombination between plasmids in mammalian cells can be enhanced by treatment of input

DNA. *Proceedings of the National Academy of Sciences*, *81*(10), 3153–3157. https://doi.org/10.1073/pnas.81.10.3153

Kim, Y. G., Cha, J., & Chandrasegaran, S. (1996). Hybrid restriction enzymes: Zinc finger fusions to Fok I cleavage domain. *Proceedings of the National Academy of Sciences*, *93*(3), 1156–1160. https://doi.org/10.1073/pnas.93.3.1156

Urnov, F. D., Rebar, E. J., Holmes, M. C., Zhang, H. S., & Gregory, P. D. (2010). Genome editing with engineered zinc finger nucleases. *Nature Reviews Genetics*, *11*(9), 636–646. https://doi.org/10.1038/nrg2842

Christian, M. L., Demorest, Z. L., Starker, C. G., Osborn, M. J., Nyquist, M. D., Zhang, Y., Carlson, D. F., Bradley, P., Bogdanove, A. J., & Voytas, D. F. (2012). Targeting G with TAL Effectors: A Comparison of Activities of TALENs Constructed with NN and NK Repeat Variable Di-Residues. *PLoS ONE*, *7*(9), e45383. https://doi.org/10.1371/journal.pone.0045383

Bogdanove, A. J., & Voytas, D. F. (2011). TAL Effectors: Customizable Proteins for DNA Targeting. *Science*, *333*(6051), 1843–1846. https://doi.org/10.1126/science.1204094

Cong, L., Ran, F. A., Cox, D., Lin, S., Barretto, R., Habib, N., Hsu, P. D., Wu, X., Jiang, W., Marraffini, L. A., & Zhang, F. (2013). Multiplex Genome Engineering Using CRISPR/Cas Systems. *Science*, *339*(6121), 819–823. https://doi.org/10.1126/science.1231143

Mali, P., Yang, L., Esvelt, K. M., Aach, J., Guell, M., DiCarlo, J. E., Norville, J. E., & Church, G. M. (2013). RNA-Guided Human Genome Engineering via Cas9. *Science*, *339*(6121), 823–826. https://doi.org/10.1126/science.1232033

Jinek, M., Chylinski, K., Fonfara, I., Hauer, M., Doudna, J. A., & Charpentier, E. (2012). A Programmable Dual-RNA–Guided DNA Endonuclease in Adaptive Bacterial Immunity. *Science*, *337*(6096), 816–821. https://doi.org/10.1126/science.1225829

Nishimasu, H., Ran, F. A., Hsu, P. D., Konermann, S., Shehata, S. I., Dohmae, N., Ishitani, R., Zhang, F., & Nureki, O. (2014). Crystal Structure of Cas9 in Complex with Guide RNA and Target DNA. *Cell*, *156*(5), 935–949. https://doi.org/10.1016/j.cell.2014.02.001

Chen, E., Lin-Shiao, E., Trinidad, M., Saffari Doost, M., Colognori, D., & Doudna, J. A. (2022). Decorating chromatin for enhanced genome editing using CRISPR-Cas9. *Proceedings of the*

National Academy of Sciences, *119*(49), e2204259119. https://doi.org/10.1073/pnas.2204259119

Chen, M., & Qi, L. S. (2017). Repurposing CRISPR System for Transcriptional Activation. In L.-C. Li (Ed.), *RNA Activation* (Vol. 983, pp. 147–157). Springer Singapore. https://doi.org/10.1007/978-981-10-4310-9_10

Qi, L. S., Larson, M. H., Gilbert, L. A., Doudna, J. A., Weissman, J. S., Arkin, A. P., & Lim, W. A. (2013). Repurposing CRISPR as an RNA-Guided Platform for Sequence-Specific Control of Gene Expression. *Cell*, *152*(5), 1173–1183. https://doi.org/10.1016/j.cell.2013.02.022

Park, J., Yoon, J., Kwon, D., Han, M.-J., Choi, S., Park, S., Lee, J., Lee, K., Lee, J., Lee, S., Kang, K.-S., & Choe, S. (2021). Enhanced genome editing efficiency of CRISPR PLUS: Cas9 chimeric fusion proteins. *Scientific Reports*, *11*(1), 16199. https://doi.org/10.1038/s41598-021-95406-8

Gaudelli, N. M., Komor, A. C., Rees, H. A., Packer, M. S., Badran, A. H., Bryson, D. I., & Liu, D. R. (2017). Programmable base editing of A•T to G•C in genomic DNA without DNA cleavage. *Nature*, *551*(7681), 464–471. https://doi.org/10.1038/nature24644

Komor, A. C., Kim, Y. B., Packer, M. S., Zuris, J. A., & Liu, D. R. (2016). Programmable editing of a target base in genomic DNA without double-stranded DNA cleavage. *Nature*, *533*(7603), 420–424. https://doi.org/10.1038/nature17946

Goswami, R., Subramanian, G., Silayeva, L., Newkirk, I., Doctor, D., Chawla, K., Chattopadhyay, S., Chandra, D., Chilukuri, N., & Betapudi, V. (2019). Gene Therapy Leaves a Vicious Cycle. *Frontiers in Oncology*, *9*, 297. https://doi.org/10.3389/fonc.2019.00297

Friedmann, T. (1992). A brief history of gene therapy. *Nature Genetics*, *2*(2), 93–98. https://doi.org/10.1038/ng1092-93

Cline, M. J., Stang, H., Mercola, K., Morse, L., Ruprecht, R., Browne, J., & Salser, W. (1980). Gene transfer in intact animals. *Nature*, *284*(5755), 422–425. https://doi.org/10.1038/284422a0

Mitchell, M. J., Billingsley, M. M., Haley, R. M., Wechsler, M. E., Peppas, N. A., & Langer, R. (2021). Engineering precision nanoparticles for drug delivery. *Nature Reviews Drug Discovery*, *20*(2), 101–124. https://doi.org/10.1038/s41573-020-0090-8

Thomas, C. E., Ehrhardt, A., & Kay, M. A. (2003). Progress and problems with the use of viral

vectors for gene therapy. *Nature Reviews Genetics*, *4*(5), 346–358. https://doi.org/10.1038/nrg1066

Shimotohno, K., & Temin, H. M. (1981). Formation of infectious progeny virus after insertion of herpes simplex thymidine kinase gene into DNA of an avian retrovirus. *Cell*, *26*(1 Pt 1), 67–77. https://doi.org/10.1016/0092-8674(81)90034-9

Wei, C. M., Gibson, M., Spear, P. G., & Scolnick, E. M. (1981). Construction and isolation of a transmissible retrovirus containing the src gene of Harvey murine sarcoma virus and the thymidine kinase gene of herpes simplex virus type 1. *Journal of Virology*, *39*(3), 935–944. https://doi.org/10.1128/jvi.39.3.935-944.1981

Tabin, C. J., Bradley, S. M., Bargmann, C. I., Weinberg, R. A., Papageorge, A. G., Scolnick, E. M., Dhar, R., Lowy, D. R., & Chang, E. H. (1982). Mechanism of activation of a human oncogene. *Nature*, *300*(5888), 143–149. https://doi.org/10.1038/300143a0

Jolly, D. J., Esty, A. C., Subramani, S., Friedmann, T., & Verma, I. M. (1983). Elements in the long terminal repeat of murine retroviruses enhance stable transformation by thymidine Idnase gene. *Nucleic Acids Research*, *11*(6), 1855–1872. https://doi.org/10.1093/nar/11.6.1855

Miller, A. D., Jolly, D. J., Friedmann, T., & Verma, I. M. (1983). A transmissible retrovirus expressing human hypoxanthine phosphoribosyltransferase (HPRT): Gene transfer into cells obtained from humans deficient in HPRT. *Proceedings of the National Academy of Sciences*, *80*(15), 4709–4713. https://doi.org/10.1073/pnas.80.15.4709

Willis, R. C., Jolly, D. J., Miller, A. D., Plent, M. M., Esty, A. C., Anderson, P. J., Chang, H. C., Jones, O. W., Seegmiller, J. E., & Friedmann, T. (1984). Partial phenotypic correction of human Lesch-Nyhan (hypoxanthine-guanine phosphoribosyltransferase-deficient) lymphoblasts with a transmissible retroviral vector. *Journal of Biological Chemistry*, *259*(12), 7842–7849. https://doi.org/10.1016/S0021-9258(17)42870-5

Bennett, J., Tanabe, T., Sun, D., Zeng, Y., Kjeldbye, H., Gouras, P., & Maguire, A. M. (1996). Photoreceptor cell rescue in retinal degeneration (rd) mice by in vivo gene therapy. *Nature Medicine*, *2*(6), 649–654. https://doi.org/10.1038/nm0696-649

Ali, R. R., Sarra, G.-M., Stephens, C., Alwis, M. D., Bainbridge, J. W. B., Munro, P. M., Fauser, S., Reichel, M. B., Kinnon, C., Hunt, D. M., Bhattacharya, S. S., & Thrasher, A. J. (2000). Restoration

of photoreceptor ultrastructure and function in retinal degeneration slow mice by gene therapy. *Nature Genetics*, *25*(3), 306–310. https://doi.org/10.1038/77068

Boughman, J. A., Vernon, M., & Shaver, K. A. (1983). Usher syndrome: Definition and estimate of prevalence from two high-risk populations. *Journal of Chronic Diseases*, *36*(8), 595–603. https://doi.org/10.1016/0021-9681(83)90147-9

Graefe, V. (1858). Exceptionelles verrhalten des gesichtsfeldes bei pigmentenartung der netzhaut. *Von Graefe's Arch Ophtlalmol*, *4*, 250-253.

Liebreich R. Abkunft aus Ehen unter Blutsverwandten als Grund von Retinitis pigmentosa. *Deutsch Klin*. 1861;13:53–55.

Usher C. H. (1914). On the inheritance of retinitis pigmentosa, with notes of cases. *Roy Land Ophthalmol Hosp Rep* 19: 130-236.

Davenport, S.L.H., Omenn, G.S., (1977). The heterogeneity of Usher syndrome. Vth Int. Conf. Birth Defects, Montreal; Petit, C., 2001. Usher syndrome: from genetics to pathogenesis. *Annu. Rev. Genomics Hum. Genet.*, 2, 271-297.

Kimberling, W. J., Moller, C. G., Reardon, W., Weston, M. D., Kenyon, J. B., Grunkemeyer, J. A., & Piekedane, S. (1992). *Linkage of Usher Syndrome Type I Gene (USHIB) to the Long Arm of Chromosome* 11. *Genomics*, *14*(4), 988–994. https://doi.org/10.1016/s0888-7543(05)80121-1

Smith, R. J. H., Lee, E. C., Kimberling, W. J., Daiger, S. P., Pelias, M. Z., Keats, B. J. B., Jay, M., Bird, A., Reardon, W., Guest, M., Ayyagari, R., & Fielding Hejtmancik, J. (1992). Localization of two genes for usher syndrome type I to chromosome 11. *Genomics*, *14*(4), 995–1002. https://doi.org/10.1016/S0888-7543(05)80122-3

Wayne, S. (1996). Localization of the Usher syndrome type ID gene (Ush1D) to chromosome 10. *Human Molecular Genetics*, *5*(10), 1689–1692. https://doi.org/10.1093/hmg/5.10.1689

Chaib, H. (1997). A newly identified locus for Usher syndrome type I, USH1E, maps to chromosome 21q21. *Human Molecular Genetics*, *6*(1), 27–31. https://doi.org/10.1093/hmg/6.1.27

Wayne, S., Lowry, R.B., McLeod, D. R., Knaus, R., Farr, C., Smith R. J. H. (1997). Localization of the Usher syndrome type IF (Ush1F) to chromosome 10*. Am J Hum Genet Suppl* 61:1752

Weil, D. (2003). Usher syndrome type I G (USH1G) is caused by mutations in the gene encoding SANS, a protein that associates with the USH1C protein, harmonin. *Human Molecular Genetics*, *12*(5), 463–471. https://doi.org/10.1093/hmg/ddg051

Kikkawa, Y. (2003). Mutations in a new scaffold protein Sans cause deafness in Jackson shaker mice. *Human Molecular Genetics*, *12*(5), 453–461. https://doi.org/10.1093/hmg/ddg042

Kimberling, J., Weston, M. D., Mijller, C., Shugart, Y. Y., Priluck, I. A., Martini, A., & Smithy, R. J. (1990). Localization of Usher Syndrome Type II to Chromosome Iq. *Genomics*, *7*(2), 245–249. https://doi.org/10.1016/0888-7543(90)90546-7

Lewis, R. A., Otterud, B., Stauffer, D., Lalouel, J.-M., & Leppert, M. (1990). Mapping recessive ophthalmic diseases: Linkage of the locus for Usher syndrome type II to a DNA marker on chromosome 1q. *Genomics*, *7*(2), 250–256. https://doi.org/10.1016/0888-7543(90)90547-8

Weston, M. D., Luijendijk, M. W. J., Humphrey, K. D., Möller, C., & Kimberling, W. J. (2004). Mutations in the VLGR1 Gene Implicate G-Protein Signaling in the Pathogenesis of Usher Syndrome Type II. *The American Journal of Human Genetics*, *74*(2), 357–366. https://doi.org/10.1086/381685

Ebermann, I., Scholl, H. P. N., Charbel Issa, P., Becirovic, E., Lamprecht, J., Jurklies, B., Millán, J. M., Aller, E., Mitter, D., & Bolz, H. (2007). A novel gene for Usher syndrome type 2: Mutations in the long isoform of whirlin are associated with retinitis pigmentosa and sensorineural hearing loss. *Human Genetics*, *121*(2), 203–211. https://doi.org/10.1007/s00439-006-0304-0

Sankila, E.-M., Pakarinen, L., Kaariainen, H., Aittomaki, K., Karjalainen, S., Sistonen, P., & De La Chapelle, A. (1995). Assignment of an Usher syndrome type III (USH3) gene to chromosome 3q. *Human Molecular Genetics*, *4*(1), 93–98. https://doi.org/10.1093/hmg/4.1.93

Namburi, P., Ratnapriya, R., Khateb, S., Lazar, C. H., Kinarty, Y., Obolensky, A., Erdinest, I., Marks-Ohana, D., Pras, E., Ben-Yosef, T., Newman, H., Gross, M., Swaroop, A., Banin, E., & Sharon, D. (2016). Bi-allelic Truncating Mutations in CEP78 , Encoding Centrosomal Protein 78, Cause Cone-Rod Degeneration with Sensorineural Hearing Loss. *The American Journal of Human Genetics*, *99*(3), 777–784. https://doi.org/10.1016/j.ajhg.2016.07.010

Puffenberger, E. G., Jinks, R. N., Sougnez, C., Cibulskis, K., Willert, R. A., Achilly, N. P., Cassidy, R. P., Fiorentini, C. J., Heiken, K. F., Lawrence, J. J., Mahoney, M. H., Miller, C. J., Nair, D. T., Politi,

K. A., Worcester, K. N., Setton, R. A., DiPiazza, R., Sherman, E. A., Eastman, J. T., … Strauss, K. A. (2012). Genetic Mapping and Exome Sequencing Identify Variants Associated with Five Novel Diseases. *PLoS ONE*, *7*(1), e28936. https://doi.org/10.1371/journal.pone.0028936

Ebermann, I., Phillips, J. B., Liebau, M. C., Koenekoop, R. K., Schermer, B., Lopez, I., Schäfer, E., Roux, A.-F., Dafinger, C., Bernd, A., Zrenner, E., Claustres, M., Blanco, B., Nürnberg, G., Nürnberg, P., Ruland, R., Westerfield, M., Benzing, T., & Bolz, H. J. (2010). PDZD7 is a modifier of retinal disease and a contributor to digenic Usher syndrome. *Journal of Clinical Investigation*, *120*(6), 1812–1823. https://doi.org/10.1172/JCI39715

Eisenberger, T., Slim, R., Mansour, A., Nauck, M., Nürnberg, G., Nürnberg, P., Decker, C., Dafinger, C., Ebermann, I., Bergmann, C., & Bolz, H. J. (2012). Targeted next-generation sequencing identifies a homozygous nonsense mutation in ABHD12, the gene underlying PHARC, in a family clinically diagnosed with Usher syndrome type 3. *Orphanet Journal of Rare Diseases*, *7*(1), 59. https://doi.org/10.1186/1750-1172-7-59

Khateb, S., Zelinger, L., Mizrahi-Meissonnier, L., Ayuso, C., Koenekoop, R. K., Laxer, U., Gross, M., Banin, E., & Sharon, D. (2014). A homozygous nonsense CEP250 mutation combined with a heterozygous nonsense C2orf71 mutation is associated with atypical Usher syndrome. *Journal of medical genetics*, *51*(7), 460–469.

Ahmed, Z. M., Jaworek, T. J., Sarangdhar, G. N., Zheng, L., Gul, K., Khan, S. N., Friedman, T. B., Sisk, R. A., Bartles, J. R., Riazuddin, S., & Riazuddin, S. (2018). Inframe deletion of human *ESPN* is associated with deafness, vestibulopathy and vision impairment. *Journal of Medical Genetics*, *55*(7), 479–488. https://doi.org/10.1136/jmedgenet-2017-105221

Riazuddin, S., Belyantseva, I. A., Giese, A. P. J., Lee, K., Indzhykulian, A. A., Nandamuri, S. P., Yousaf, R., Sinha, G. P., Lee, S., Terrell, D., Hegde, R. S., Ali, R. A., Anwar, S., Andrade-Elizondo, P. B., Sirmaci, A., Parise, L. V., Basit, S., Wali, A., Ayub, M., … Ahmed, Z. M. (2012). Alterations of the CIB2 calcium- and integrin-binding protein cause Usher syndrome type 1J and nonsyndromic deafness DFNB48. *Nature Genetics*, *44*(11), 1265–1271. https://doi.org/10.1038/ng.2426

Khateb, S., Zelinger, L., Mizrahi-Meissonnier, L., Ayuso, C., Koenekoop, R. K., Laxer, U., Gross, M., Banin, E., & Sharon, D. (2014). A homozygous nonsense CEP250 mutation combined with a heterozygous nonsense C2orf71 mutation is associated with atypical Usher syndrome. *Journal of medical genetics*, *51*(7), 460–469.

Nolen, R. M., Hufnagel, R. B., Friedman, T. B., Turriff, A. E., Brewer, C. C., Zalewski, C. K., King, K. A., Wafa, T. T., Griffith, A. J., Brooks, B. P., & Zein, W. M. (2020). Atypical and ultra-rare Usher syndrome: A review. *Ophthalmic Genetics*, *41*(5), 401–412. https://doi.org/10.1080/13816810.2020.1747090

Reiners, J., Van Wijk, E., Märker, T., Zimmermann, U., Jürgens, K., Te Brinke, H., Overlack, N., Roepman, R., Knipper, M., Kremer, H., & Wolfrum, U. (2005). Scaffold protein harmonin (USH1C) provides molecular links between Usher syndrome type 1 and type 2. *Human Molecular Genetics*, *14*(24), 3933–3943. https://doi.org/10.1093/hmg/ddi417

Reiners, J., Van Wijk, E., Märker, T., Zimmermann, U., Jürgens, K., Te Brinke, H., Overlack, N., Roepman, R., Knipper, M., Kremer, H., & Wolfrum, U. (2005). Scaffold protein harmonin (USH1C) provides molecular links between Usher syndrome type 1 and type 2. *Human Molecular Genetics*, *14*(24), 3933–3943. https://doi.org/10.1093/hmg/ddi417

Reiners, J., Nagel-Wolfrum, K., Jürgens, K., Märker, T., & Wolfrum, U. (2006). Molecular basis of human Usher syndrome: Deciphering the meshes of the Usher protein network provides insights into the pathomechanisms of the Usher disease. *Experimental Eye Research*, *83*(1), 97–119. https://doi.org/10.1016/j.exer.2005.11.010

Kremer, H., Van Wijk, E., Märker, T., Wolfrum, U., & Roepman, R. (2006). Usher syndrome: Molecular links of pathogenesis, proteins and pathways. *Human Molecular Genetics*, *15*(suppl_2), R262–R270. https://doi.org/10.1093/hmg/ddl205

El-Amraoui, A., & Petit, C. (2005). Usher I syndrome: Unravelling the mechanisms that underlie the cohesion of the growing hair bundle in inner ear sensory cells. *Journal of Cell Science*, *118*(20), 4593–4603. https://doi.org/10.1242/jcs.02636

Adato, A., Michel, V., Kikkawa, Y., Reiners, J., Alagramam, K. N., Weil, D., Yonekawa, H., Wolfrum, U., El-Amraoui, A., & Petit, C. (2005). Interactions in the network of Usher syndrome type 1 proteins. *Human Molecular Genetics*, *14*(3), 347–356. https://doi.org/10.1093/hmg/ddi031

Maerker, T., Van Wijk, E., Overlack, N., Kersten, F. F. J., McGee, J., Goldmann, T., Sehn, E., Roepman, R., Walsh, E. J., Kremer, H., & Wolfrum, U. (2008). A novel Usher protein network at the periciliary reloading point between molecular transport machineries in vertebrate photoreceptor cells. *Human Molecular Genetics*, *17*(1), 71–86. https://doi.org/10.1093/hmg/ddm285

Tian, G., Zhou, Y., Hajkova, D., Miyagi, M., Dinculescu, A., Hauswirth, W. W., Palczewski, K., Geng, R., Alagramam, K. N., Isosomppi, J., Sankila, E.-M., Flannery, J. G., & Imanishi, Y. (2009). Clarin-1, Encoded by the Usher Syndrome III Causative Gene, Forms a Membranous Microdomain. *Journal of Biological Chemistry*, *284*(28), 18980–18993. https://doi.org/10.1074/jbc.M109.003160

Weson, M. D., Kelley, P. M., Overbeck, L. D., Orten, D. J., & Hasson, T. (1996). Myosin VIIA Mutation Screening in 189 Usher Syndrome Type 1 Patients. *American journal of human genetics*, *59*(5), 1074–1083.

Adato, A., Weil, D., Kalinski, H., Pel-Or, Y., Ayadi, H., Petit, C., Korostishevsky, M., & Bonne-Tamir, B. (1997). Mutation Profile of All 49 Exons of the Human Myosin VIIA Gene, and Haplotype Analysis, in Usher 1B Families from Diverse Origins. *The American Journal of Human Genetics*, *61*(4), 813–821. https://doi.org/10.1086/514899

Ouyang, X.M., Yan, D., Du, L.L. *et al.* Characterization of Usher syndrome type I gene mutations in an Usher syndrome patient population. *Hum Genet* 116, 292–299 (2005). https://doi.org/10.1007/s00439-004-1227-2

Riazuddin, S., Nazli, S., Ahmed, Z. M., Yang, Y., Zulfiqar, F., Shaikh, R. S., Zafar, A. U., Khan, S. N., Sabar, F., Javid, F. T., Wilcox, E. R., Tsilou, E., Boger, E. T., Sellers, J. R., Belyantseva, I. A., Riazuddin, S., & Friedman, T. B. (2008). Mutation spectrum of MYO7A and evaluation of a novel nonsyndromic deafness DFNB2 allele with residual function. *Human mutation*, *29*(4), 502–511. https://doi.org/10.1002/humu.20677

Jaijo, T., Aller, E., Beneyto, M., Najera, C., Graziano, C., Turchetti, D., Seri, M., Ayuso, C., Baiget, M., Moreno, F., Morera, C., Perez-Garrigues, H., & Millan, J. M. (2006). MYO7A mutation screening in Usher syndrome type I patients from diverse origins. *Journal of Medical Genetics*, *44*(3), e71–e71. https://doi.org/10.1136/jmg.2006.045377

Jacobson, S. G., Cideciyan, A. V., Gibbs, D., Sumaroka, A., Roman, A. J., Aleman, T. S., Schwartz, S. B., Olivares, M. B., Russell, R. C., Steinberg, J. D., Kenna, M. A., Kimberling, W. J., Rehm, H. L., & Williams, D. S. (2011). Retinal Disease Course in Usher Syndrome 1B Due to *MYO7A* Mutations. *Investigative Ophthalmology & Visual Science*, *52*(11), 7924. https://doi.org/10.1167/iovs.11-8313

French, L. S., Mellough, C. B., Chen, F. K., & Carvalho, L. S. (2020). A Review of Gene, Drug and Cell-Based Therapies for Usher Syndrome. *Frontiers in Cellular Neuroscience*, *14*, 183. https://doi.org/10.3389/fncel.2020.00183

Zallocchi, M., Binley, K., Lad, Y., Ellis, S., Widdowson, P., Iqball, S., Scripps, V., Kelleher, M., Loader, J., Miskin, J., Peng, Y.-W., Wang, W.-M., Cheung, L., Delimont, D., Mitrophanous, K. A., & Cosgrove, D. (2014). EIAV-Based Retinal Gene Therapy in the shaker1 Mouse Model for Usher Syndrome Type 1B: Development of UshStat. *PLoS ONE*, *9*(4), e94272. https://doi.org/10.1371/journal.pone.0094272

Hashimoto, T., Gibbs, D., Lillo, C., Azarian, S. M., Legacki, E., Zhang, X.-M., Yang, X.-J., & Williams, D. S. (2007). Lentiviral gene replacement therapy of retinas in a mouse model for Usher syndrome type 1B. *Gene Therapy*, *14*(7), 584–594. https://doi.org/10.1038/sj.gt.3302897

Ail, D., Malki, H., Zin, E. A., & Dalkara, D. (2023). Adeno-Associated Virus (AAV) - Based Gene Therapies for Retinal Diseases: Where are We? *The Application of Clinical Genetics*, *Volume 16*, 111–130. https://doi.org/10.2147/TACG.S383453

Wu, Z., Yang, H., & Colosi, P. (2010). Effect of Genome Size on AAV Vector Packaging. *Molecular Therapy*, *18*(1), 80–86. https://doi.org/10.1038/mt.2009.255

Salganik, M., Hirsch, M. L., & Samulski, R. J. (2015). Adeno-associated Virus as a Mammalian DNA Vector. *Microbiology Spectrum*, *3*(4), 3.4.04. https://doi.org/10.1128/microbiolspec.MDNA3-0052-2014

Allocca, M., Doria, M., Petrillo, M., Colella, P., Garcia-Hoyos, M., Gibbs, D., Kim, S. R., Maguire, A., Rex, T. S., Di Vicino, U., Cutillo, L., Sparrow, J. R., Williams, D. S., Bennett, J., & Auricchio, A. (2008). Serotype-dependent packaging of large genes in adeno-associated viral vectors results in effective gene delivery in mice. *Journal of Clinical Investigation*, *118*(5), 1955–1964. https://doi.org/10.1172/JCI34316

Colella, P., Trapani, I., Cesi, G., Sommella, A., Manfredi, A., Puppo, A., Iodice, C., Rossi, S., Simonelli, F., Giunti, M., Bacci, M. L., & Auricchio, A. (2014). Efficient gene delivery to the cone-enriched pig retina by dual AAV vectors. *Gene therapy*, *21*(4), 450–456. https://doi.org/10.1038/gt.2014.8

Lau, S. C., Grati, M., Isgrig, K., Sinan, M., Calabro, K. R., Zhu, J., Ishibashi, Y., Ozgur, Z., Wafa, T., Belyantseva, I. A., Fitzgerald, T., Friedman, T. B., Boye, S. L., Boye, S. E., & Chien, W. W. (2023).

Dual-AAV vector-mediated expression of MYO7A improves vestibular function in a mouse model of Usher syndrome 1B. *Molecular Therapy - Methods & Clinical Development*, *30*, 534–545. https://doi.org/10.1016/j.omtm.2023.08.012

Zhang, H., Bamidele, N., Liu, P., Ojelabi, O., Gao, X. D., Rodriguez, T., Cheng, H., Kelly, K., Watts, J. K., Xie, J., Gao, G., Wolfe, S. A., Xue, W., & Sontheimer, E. J. (2022). Adenine Base Editing *In Vivo* with a Single Adeno-Associated Virus Vector. *GEN Biotechnology*, *1*(3), 285–299. https://doi.org/10.1089/genbio.2022.0015

Meng, J., Moore, M., Counsell, J., Muntoni, F., Popplewell, L., & Morgan, J. (2022). Optimized lentiviral vector to restore full-length dystrophin via a cell-mediated approach in a mouse model of Duchenne muscular dystrophy. *Molecular therapy. Methods & clinical development*, *25*, 491–507. https://doi.org/10.1016/j.omtm.2022.04.015

Williams, D. S., & Lopes, V. S. (2011). The many different cellular functions of MYO7A in the retina. *Biochemical Society transactions*, *39*(5), 1207–1210. https://doi.org/10.1042/BST0391207

Lau, S. C., Grati, M., Isgrig, K., Sinan, M., Calabro, K. R., Zhu, J., Ishibashi, Y., Ozgur, Z., Wafa, T., Belyantseva, I. A., Fitzgerald, T., Friedman, T. B., Boye, S. L., Boye, S. E., & Chien, W. W. (2023). Dual-AAV vector-mediated expression of *MYO7A* improves vestibular function in a mouse model of Usher syndrome 1B. *Molecular therapy. Methods & clinical development*, *30*, 534–545. https://doi.org/10.1016/j.omtm.2023.08.012

Moore, S. T., Nakamura, T., Nie, J., Solivais, A. J., Aristizábal-Ramírez, I., Ueda, Y., Manikandan, M., Reddy, V. S., Romano, D. R., Hoffman, J. R., Perrin, B. J., Nelson, R. F., Frolenkov, G. I., Chuva de Sousa Lopes, S. M., & Hashino, E. (2023). Generating high-fidelity cochlear organoids from human pluripotent stem cells. Cell stem cell, 30(7), 950–961.e7.